Assessment of Seismic Integrity of Multi-Span Curved Bridges in Mid-America

Part I: Implications of Design Assumptions on Capacity Estimates and Limit States of Multi-Span Curved Bridges

by

A.M. Mwafy and A.S. Elnashai

Mid-America Earthquake Center
Civil and Environmental Engineering Department
University of Illinois at Urbana-Champaign, IL, USA

April 2007

This research is supported by the Mid-America Earthquake Center
under National Science Foundation Grant EEC-9701785

TABLE OF CONTENTS

SUMMARY

The study presents a detailed seismic performance assessment of a complex office-designed bridge using state-of-the-art assessment tools and metrics. The impact of design assumptions on the capacity estimates and dynamic characteristics of a multi-span curved bridge are investigated. A single nine-span bridge is studied whilst the level of attention to detail is significantly higher than can be achieved in a mass parametric study of a population of bridges. The objective is achieved by in-depth investigation of the bridge representing the 'as-designed' (including features assumed in the design process) and that representing the 'as-built' (actual expected characteristics) structure. Three-dimensional detailed dynamic response simulations of the investigated bridge including soil-structure interaction effects are undertaken. The behavior of the 'as-designed' bridge is investigated on two different analytical platforms for elastic and inelastic analysis. A third idealization is adopted to investigate the 'as-built' behavior by realistically modeling bridge bearings, structural gaps and materials. A comprehensive list of local and global, action and deformation, performance indicators are selected to monitor the response to earthquake action, including bearing slippage and segment collision. The adopted methodology and results of elastic and inelastic analyses are discussed. The comparative study has indicated that the lateral capacity and dynamic characteristics of the as-designed bridge are significantly different than the as-built behavior. The potential of pushover analysis in identifying structural deficiencies, estimation of capacities and providing insight into the pertinent limit state criteria are demonstrated. The conclusions from this study are important for designers and assessors of the seismic response of complex bridges since it highlights potentially non-conservative assumptions that are frequently used in the design office.

INTRODUCTION

Multi-span highway bridges are strategic elements in modern transportation networks that warrant careful design to insure their functionality during and after earthquakes. The reliable detailed assessment of such complex structures is thus vital for deciding whether their design procedures are adequate. Reliable assessment also enables improvements in seismic performance by timely intervention. There are two bounding approaches for studying bridge structures. There are (i) extensive parametric studies that are by necessity not extremely detailed, due to the required large number of parametric variations (such as type of foundation, characteristics of piers, pier-to-deck connections, deck section properties, abutment type and deck-abutment connection), and (ii) extremely detailed analysis of a sample complex bridge that features many issues of importance to bridge system response. Both approaches are important and complementary. The current study belongs to the second class.

The proportion of horizontal-to-vertical load generally increases in continuous, joint-free, redundant structures. Hence, an efficient design and energy dissipation approach is attained by artificially increasing the period of vibration and the energy dissipated in secondary elements, thus maintaining the integrity of primary structural members. Base-isolation bridges thus exploit seismic isolation bearings and dissipation/damping devices to achieve the latter design philosophy. Elastomeric bearings can act as isolation devices to dissipate energy via their inelastic response and friction. Owing to the higher attention usually paid to primary structural members and the restriction of movement imposed at abutments, the bearing frictional resistance may be neglected in the design. This assumption may be non-conservative since PTFE bearings, which may have low friction at the low velocity rates, generate higher friction under high seismic deformation (e.g. Constantinou et al. 1990; Priestley et al. 1996). It is therefore necessary to investigate the assumptions conventionally adopted in the design and compare the ensuing behavior with more realistic simulations to assess their consequences on seismic integrity of bridge structures.

The two key elements of assessment procedures are capacity and demand. Capacity is a measure of the capability (supply) of the system to resist seismic actions, while the demand is a measure of the requirements imposed by earthquake ground motions. Pushover analysis is a powerful tool for evaluating the lateral force-resisting capacity

and may be also employed to predict the seismic demand by estimating the target displacement at the design earthquake. Several improvements have been suggested in recent years to advance pushover analysis (e.g. Elnashai 2001; Antoniou and Pinho 2004). However, newly developed procedures still do not guarantee satisfactory results with increasing input ground motions peculiarity and structural irregularity (Elnashai 2002). The more enhancements involved in new proposals may also have impact on simplicity, an important criterion for analysis procedures intended for the design office environment. Although the conventional pushover procedure is more applicable to structures mainly vibrating in their fundamental mode (Mwafy and Elnashai 2001), it has been proved valuable for capacity estimates of long period structures and highway bridges (e.g. Mwafy et al. 2006-b; Zheng et al. 2003; Lu et al. 2004). Notwithstanding, more research is still needed to investigate the applicability of pushover analysis for capacity and limit state predictions of multi-span complex bridges, particularly those with curvature, sliders and expansion joints.

The objective of this study is to investigate consequences of the design assumptions on the dynamic characteristics and capacity-demand predictions of multi-span complex bridges by comparisons with realistic simulations. The study is conducted on a 1488 feet nine-span bridge carefully selected from the Federal Highway Administration (FHWA) inventory to represent a US typical design of complex highway bridges (FHWA 1996). Extensive analyses are performed using state of the art analytical tools to verify the analytical models and to compare estimates of capacities and demands. This report focuses on the following sub-objectives: (i) present the methodology adopted to assess the seismic response of complex bridges, (ii) verify different modeling approaches and select relevant performance criteria, (iii) investigate the applicability of pushover analysis for evaluation of capacities and the controlling limit state criteria and (iv) compare the 'design assumption' and the 'as-built' configurations to evaluate impact of various modeling approaches on seismic integrity of multi-span bridges. Comparisons of the capacity with the demand obtained from response history analysis are discussed in Part II of this study.

STRUCTURAL AND GEOTECHNICAL CHARACTERISTICS

The application case study investigated herein is an US-designed multi-span bridge constructed in a medium seismicity region with PGA of 0.15g. A number of borings drilled along the bridge alignment indicated that the

subsoil is coarse alluvial flood deposits (very dense sand and gravel) for a depth of 50 feet overlying volcaniclastic sediments. The plan and elevation of the 1488 feet, nine-span bridge are shown in Figure 1. It consists of two units separated by an expansion joint: a four-span straight unit and a five-span curved one. While the two units act independently in the longitudinal direction, they are linked in transverse deformation at the intermediate expansion joint and pivoting at the abutments. The superstructure is composed of four steel girders with a composite cast-in-place concrete deck. Conventional steel pinned bearings were used at Piers 1, 2, 3, 6 and 7 to resist the seismic forces in the longitudinal direction. The bearings at the abutments, the expansion joint and at Piers 5 and 8 are PTFE sliders providing restraint in the transverse direction only. Elastomeric bearings with a stainless steel sliding surface were employed for all movable bearings. The transverse resistance is provided via girder stops capable of transferring transverse forces. The seat-type abutments and the single-column intermediate piers are all cast-in-place and supported on steel H-piles.

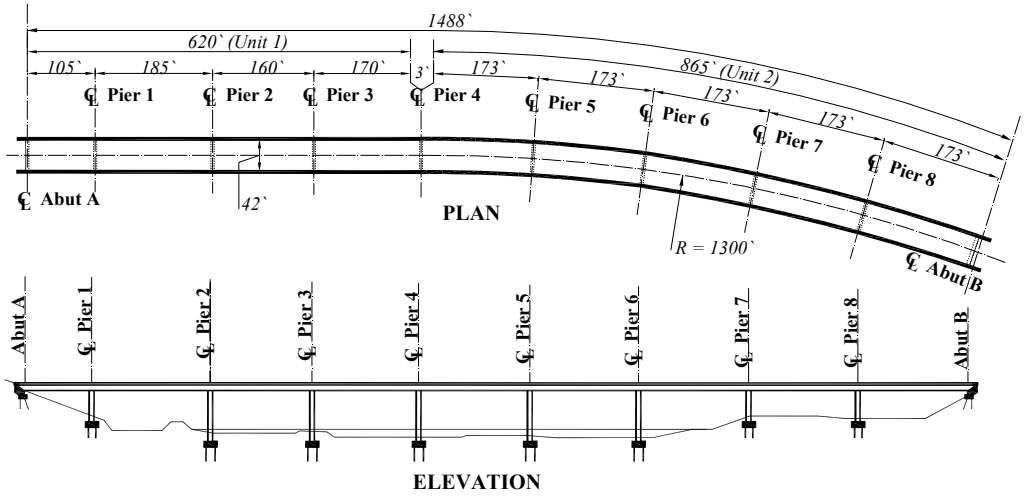

Figure 1. The FHWA nine-span steel-girder bridge.

The design of the bridge conforms to the AASHTO Standard Specifications (1995). Since the bridge crosses the main channel of a wide river, flow and ice loading dictated the dimensions of piers. The case study thus exemplifies a bridge controlled by segment collision and deformation rather than ductility and strength limit state criteria, as subsequently discussed. This emphasizes the significance of different performance indicators in seismic design and assessment of bridges. Furthermore, in view of recent changes in the US seismic hazard (USGS 2002) the selection of this design example was motivated by the desire to investigate the vulnerability of complex bridges in medium

seismicity regions under higher levels of ground motions than the design earthquake. Further structural detailing and geotechnical information are provided elsewhere (FHWA 1996).

STRUCTURAL AND FOUNDATION MODELING

Refined three-dimensional models of the entire bridge including foundations and soil effect were assembled for elastic and inelastic analysis using SAP2000 (CSI 2003) and Zeus-NL (Elnashai et al. 2004), respectively. The former modeling approach was employed for verifications of the Zeus-NL fiber modeling with the design before executing the extensive inelastic analysis. Zeus-NL is mainly employed to estimate the capacities and demands from inelastic pushover and response history analysis. The latter finite element analysis platform was developed and thoroughly tested at Imperial College, UK, (Izzuddin and Elnashai 1989). The further development and verification of the program with full scale test results have continued at University Illinois at Urbana-Champaign, USA, to deliver a state-of-the-art inelastic analytical platform for static and dynamic analysis of steel, concrete and composite structures (e.g. Jeong and Elnashai 2005).

In the detailed Zeus-NL modeling, each structural member is assembled using a number of cubic elasto-plastic elements capable of representing the spread of inelasticity within the member cross-section and along the member length via the fiber analysis approach. Sections are discretized to steel, confined and unconfined concrete fibers. The stress-strain response at each fiber is monitored during the entire multi-step analysis. Gravity loads and mass are distributed on the superstructure and along the height of piers. The employed distributed mass elements utilize cubic shape function and account for both the translational and rotational inertia. Figures 2 and 3 depict the Zeus-NL modeling approach of the superstructure and the entire bridge, respectively. Modeling of the pier and its connection to the superstructure and the foundation system is described in Figure 3(c). A number of modeling approaches were extensively investigated to select rational idealizations of superstructure, materials and bearings, as discussed below.

Superstructure and Material Modeling

Modern seismic design philosophy of bridges relies on piers to dissipate energy rather than the superstructure, which remains elastic under the design earthquake. Based on the conventional elastic theory, the superstructure is

modeled using three different cross sections; two hollow steel box sections equivalent to the four steel girders and a RC rectangular cross section representing the deck. This conforms to the following two criteria: (i) equal sectional areas and (ii) equivalent sectional moments of inertia and torsional constant. It is important to note that the total torsional resistance of the employed closed steel cross sections is higher than those of the four steel girders. However, the steel cross frames, employed to transfer the superstructure mass to piers, increase the torsional resistance of the four steel girders. Thus, the adopted modeling approach realistically predicts the elastic behavior of the superstructure. The elements idealizing the superstructure are located at the centeroid of the cross sections and connected together using rigid arms, as shown in Figure 2.

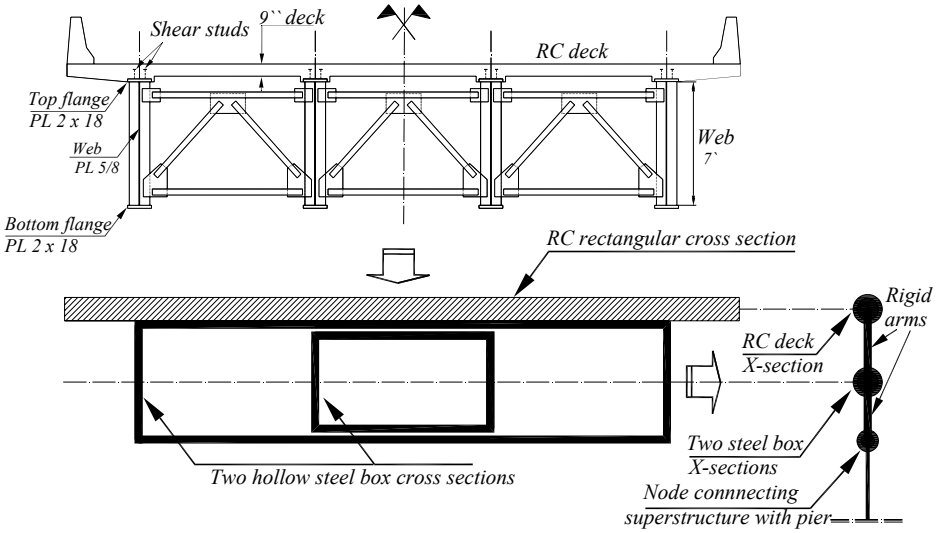

Figure 2. Modeling approach of superstructure.

On the other hand, employing the characteristic material strength causes reduction in stiffness and elongation in period. Hence, the characteristics values are only used for modeling the design configuration, while the more realistic mean values are employed to assess the response of the as-built bridge. A normal distribution is adopted to estimate the concrete compressive strength and steel yield strength. An average coefficient of variation (COV) of 12% for concrete, assuming average curing conditions and workmanship, and 6% for the steel, calculated from previous experiments, are adopted (Rossetto and Elnashai 2005).

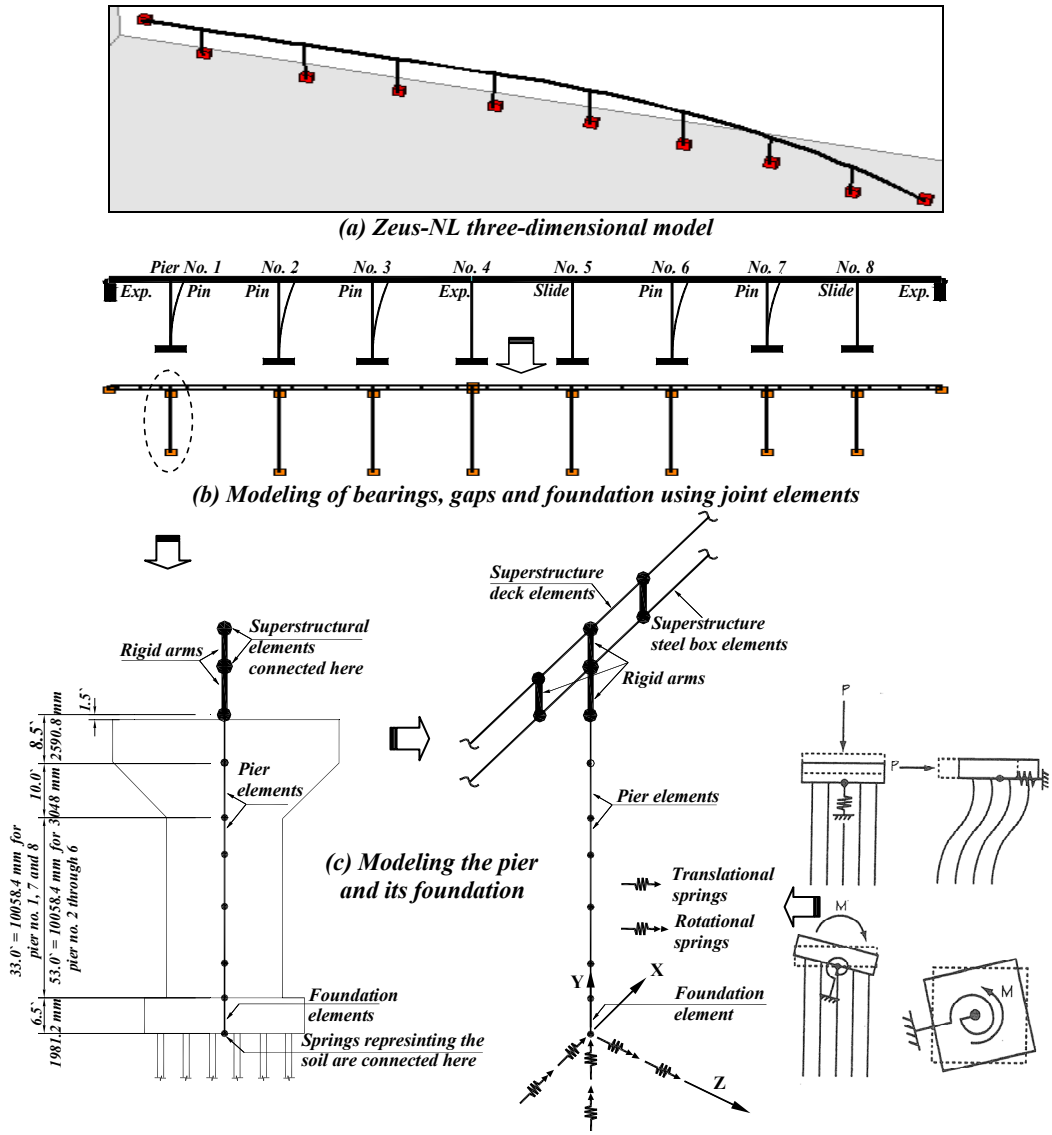

Figure 3. ZeusNL model for the nine-span bridge

Foundation Modeling

The inertial soil-structure interaction is caused by deformation of the soil by the time varying inertia induced forces developed in the footing. Based on the boring profile at the construction site, a soil type I was used in the design (AASHTO 1995). This corresponds to stable deposits of sand and gravel less than 200 feet overlying rock. The inertial soil-structure interaction is thus accounted for by restraining the pile caps with grounded springs representing the stiffness of the bridge pile foundations, as depicted in Figures 3(c) for an intermediate pier. The local coordinates of piers are used to idealize the foundation stiffness, which is calculated as follows:

- The axial and lateral stiffness of an individual pile were calculated.
- The pile group stiffnesses were obtained from combinations of individual piles.
- As a result to the high rigidity of the footing, contribution of the pile cap was neglected. This is justified by the large relative stiffness of the foundation compared with the pier. Hence, the resulting demand on the substructure will not change.
- Since the soil may not be in full contact with the pile caps, and to account for any liquefaction potential, the soil contribution was conservatively disregarded in this modeling. Constructing of the bridge in the flood plain of a large river supports this scenario due to loss of contact under the pile caps.

For the pile-bent abutment type used in the design, wing walls don't contribute much to the transverse horizontal resistance. Therefore, the transverse horizontal stiffness of the abutment is estimated using the translational stiffness of the abutment pile group. In the longitudinal direction, the abutment embankment fill stiffness is estimated based on the finding of a large-scale abutment testing (Maroney, 1995). The initial passive stiffness from this testing (11.5 kN/mm/m) is adjusted relative to the back-wall height (Caltrans, 2004). A maximum passive pressure was recommended in the latter study, allowing the back-wall to break off in order to prevent inelasticity in the foundation system. The stiffness in active action is assumed to be one fifth of the passive stiffness (Choi et al., 2004). A bilinear elasto-plastic relationship is therefore adopted to model the longitudinal behavior of the abutment. The vertical translation and torsional rotation of the abutment-superstructure connection are fully restrained, while the rotation about the transverse and vertical axis is released. The springs and releases conform to the local coordinate system of the abutments.

Bearings and Gaps Modeling

A zero frictional resistance is initially assumed at all sliding bearings with restrictions of movement at abutments. Although this idealization is rather unrealistic, it was employed to be in consistency with the assumptions made in the design phase. A rational estimation of the bearing frictional resistance is adopted afterwards in another idealization to assess the behavior of the as-built structure. The PTFE-stainless steel movable bearings used in the design have small friction coefficient at the low velocity rates (2-5%), while have higher friction under high seismic deformation. For non-lubricated bearings, this coefficient at high velocities ranges from 5 to 15%, or even higher at

the low temperature (Constantinou et al., 1990; Priestley et al., 1996; Bondonet and Filiatrault, 1997). It was also concluded in previous experimental studies that the coefficient of friction slightly decreases again under the high velocities due to frictional heating. The bridge investigated in the current study is assessed under increasing levels of input ground motion. Accordingly, it was decided to use a 10% friction coefficient for the analytical model used to assess the as-built behavior of the bridge.

Two modeling approaches were investigated to idealize the impact stiffness. In the first approach, the pounding is represented by a nonlinear spring (Hertz model). The impact stiffness increases in this approach from 2.92E6 MPa to 4.38E6 MPa at a penetration of 1.27 mm, and increases again at 2.54 mm to 8.76E6 MPa (e.g. Choi et al., 2004). These values are controlled to ensure that the penetration of pounding is less than 2.54 mm (0.1 in). Muthukumar and DesRoches (2006) concluded that this modeling approach is sufficient for the impact simulation at a PGA of 0.1-0.3g, which is the intensity range investigated in the present study. Results obtained from this idealization were compared with a more simplified linear spring model employing the maximum impact stiffness (Ki) of 8.76E6 MPa. It was concluded that the former model has insignificant effect on the response at the design earthquake, while it has a marginal effect at twice the design earthquake, compared with the simplified linear model. It was therefore decided to use the simplified approach to model the impact stiffness. Figure 4 shows the force versus relative displacement relationships of the joint elements representing the expansion joint, movable bearings and structural gaps. In this modeling, a positive relative displacement corresponds to an opening of the joint gap and a negative displacement corresponds to a closing of the gap. When the gap at the abutment and at the expansion joint undergoes a relative movement in the negative direction (joint close) exceeding the gap width, the joint element begins resisting further opening (collisions). It is clear that slippage takes place in the as-built modeling when the applied force reaches the maximum friction developed on the contact plane of the bearing.

LIMIT STATES AND ANALYSIS PROCEDURE

The performance criteria for yield and collapse are classified into two groups (Mwafy and Elnashai 2001 and 2002): local (member level) and global (structure level) criteria. Member yield is considered when the strain in the main longitudinal tensile reinforcement exceeds the steel yield strain. The yield limit state on the structure level is

estimated from an elasto-plastic idealization of the lateral response. On the other hand, exceeding the ultimate curvature is considered as the local failure criteria. This is controlled by the ultimate compression strain of the confined concrete at the extreme fiber (ε_{cu}), which is estimated according to the level of confinement. By considering overall structural characteristics, the following criteria are utilized to define global failure: (i) excessive drift of 3.0%; (ii) significant degradation of lateral strength of more than 10%; (iii) slippage (unseating) or collision failure at the abutments or the expansion joint; and (iv) formation of a hinging mechanism. The gap elements employed at the expansion joint and at the abutments allow for predicting possible unseating or bounding between different structural segments, as indicated in Figure 4. To obtain complete capacity envelopes of the structure and its piers, the gap elements are not included in pushover analysis.

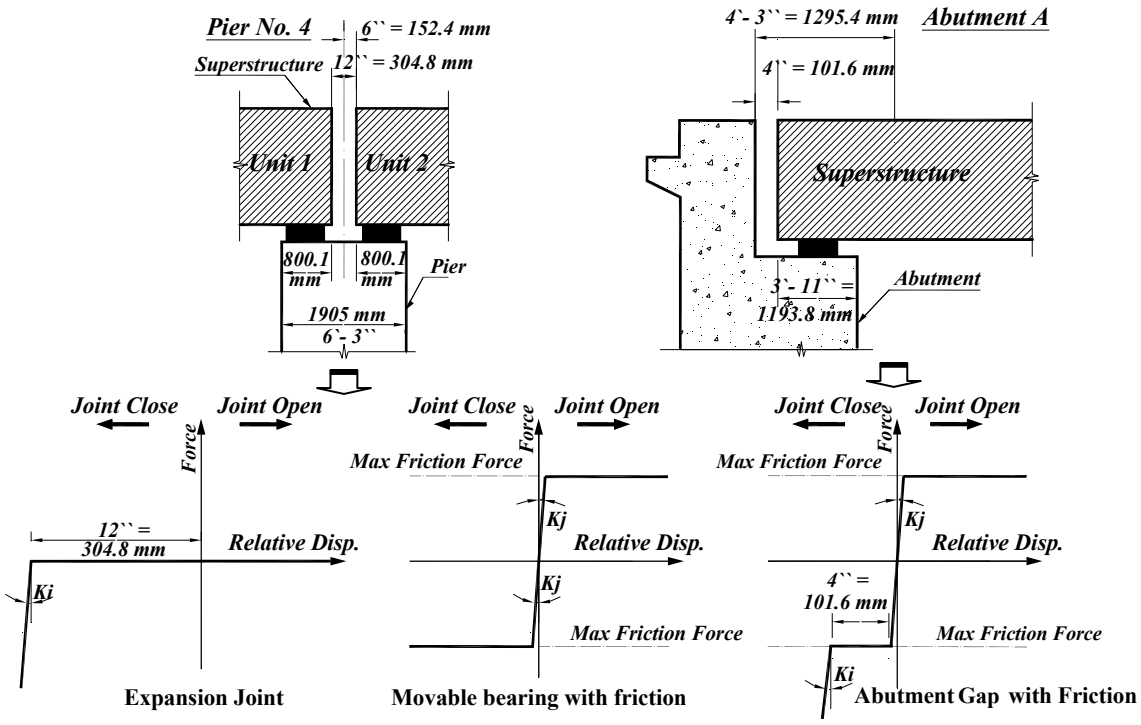

Figure 4. Force-displacement relationships of the joint elements representing the expansion joint and abutment gaps.

Formation of a hinging collapse mechanism represents a state of failure. In the transverse direction, such a mechanism involves plastic hinges at extremities of all piers. In the other direction, piers are connected to the superstructure via pinned or movable bearings. Hence, a sway mechanism may occur due to formation of plastic

hinges at the base of Piers 1, 2 and 3 for Unit 1, or Piers 6 and 7 for Unit 2, as shown from Figure 5. Although the structure is more vulnerable to this failure mechanism in the longitudinal direction, the controlled deformation at the expansion joint and at the abutments is intended to prevent this mechanism. To employ this limit state criterion, inelastic pushover analysis is conducted first up to the collapse drift limit state to investigate the vulnerability of the structure to such mechanism. Observing this mechanism is an indication of the vulnerability of the system, leading to considering it in response history analysis. This approach is undertaken to avoid the over-conservatism since plastic hinges involved in this mechanism do not form simultaneously in response history analysis. The structure is also assumed to have failed if the steel strain of both sides of all piers cross sections exceeded the yield strain.

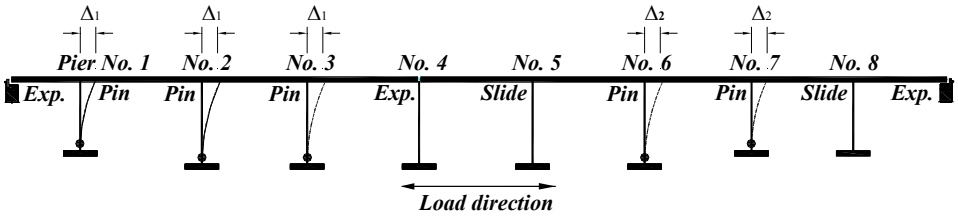

Figure 5. Definition of the sway collapse mechanism in the longitudinal directions for the bridge featuring the assumptions considered in the design.

SAP2000 and Zeus-NL are employed to assess the elastic and inelastic response of the design and the as-built models. Eigenvalue analysis is first conducted to determine the un-cracked horizontal and vertical periods of vibration and mode shapes. This analysis is used to verify the analytical models by comparisons between results of the aforementioned two analytical tools. Response spectrum analysis is then carried out using the design spectrum to compare the design response parameters with the capacities estimated from pushover analysis and the demands predicted from response history analysis. Applicability of the pushover analysis procedure for evaluation of the global behavior, monitoring the spread of yielding and detecting undesirable failure modes in then investigated. The analysis of the entire bridge is performed in both the longitudinal and transverse directions using invariant lateral load distributions calculated from combinations of various modes of vibrations. Pushover analysis is considered the final verification tool for the proposed models prior to executing the response history analysis. The latter analysis is finally performed to examine the response of the structures under a set of synthetic ground motions representing the

site. The comprehensive results of response history analyses are presented in Part II of this study and by Mwafy et al. (2006-a), while other analysis results are discussed below.

DYNAMIC CHARACTERISTICS AND MODEL VERIFICATION

Comparisons between the modes of vibration of the design configuration obtained from SAP2000 and Zeus-NL are given in Figures 6 and 7(a), respectively. It is clear that the mode shapes of both analytical platforms are comparable. The first and second mode shapes are in the longitudinal direction for unit 2 and 1, respectively. The predominant mode in the transverse direction is the third mode. For this modeling approach, which disregards friction, it is confirmed that the two units of the structure independently vibrate in the longitudinal direction. The stiffness of Unit 1 is higher than Unit 2 in this direction as a result of the participation of three piers in resisting the inertia forces transmitted from the superstructure. This is unlike the case of Unit 2 since two piers only resist the longitudinal seismic forces.

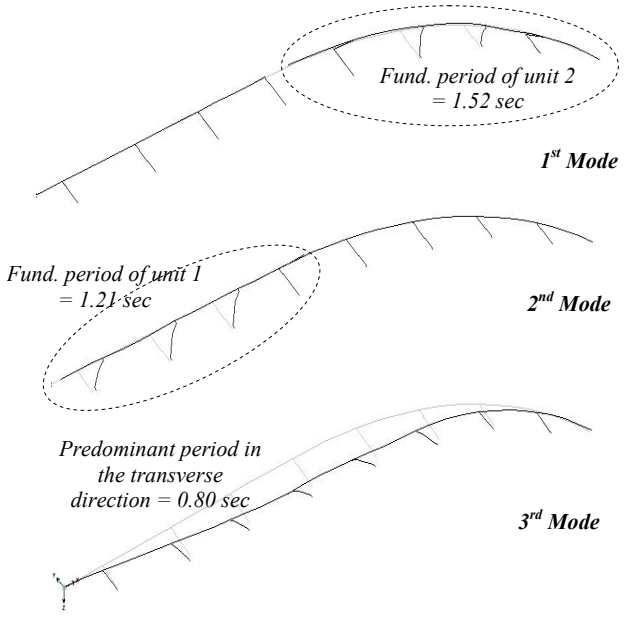

Figure 6. SAP2000 dynamic characteristics of the bridge featuring the assumptions considered in the design.

The periods obtained from Zeus-NL are slightly lower than those from SAP2000 due to the difference between the superstructure modeling approach adopted in the two programs. Following the design assumptions, the SAP2000 model employs an equivalent RC cross section, in which the cross-sectional area of the steel girders was

transformed to a concrete section using the modular ratio. Also the concrete deck was only considered to estimate the torsional rigidity. Since this assumption underestimates the superstructure geometrical properties, Zeus-NL modeling employs a more rational idealization, as discussed earlier (refer to Figure 2). Therefore, Zeus-NL results are in principle more realistic compared with those obtained from the SAP2000.

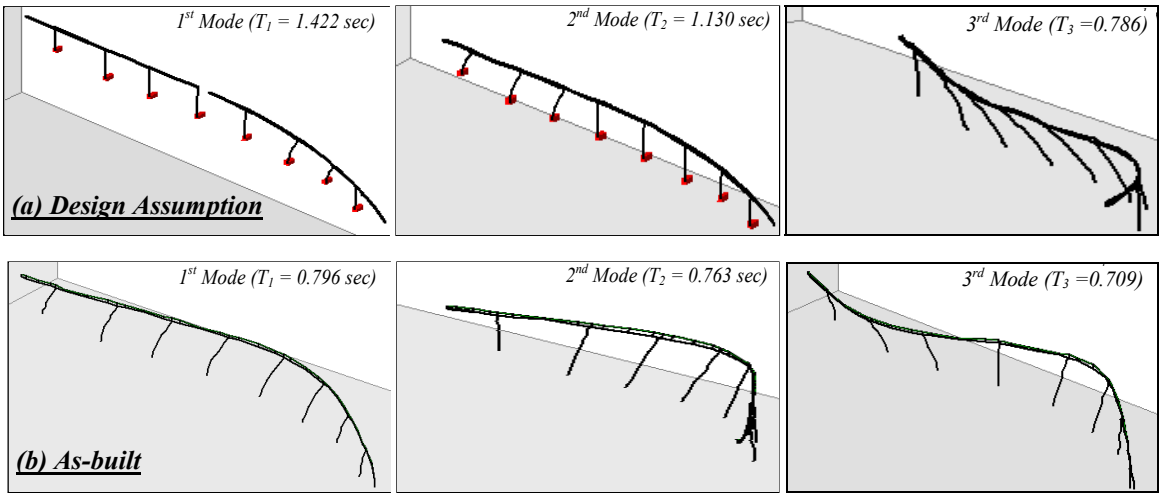

Figure 7. Zeus-NL dynamic characteristics for (a) the bridge featuring the assumptions considered in the design and (b) the as-built configuration with bearing friction.

Comparison of the dynamic characteristics of the design assumption and the as-built bridge models is shown in Figure 7. It is clear that the behavior is significantly and fundamentally affected when considering friction. The fundamental period decreases by about 50% and the modes of vibration are altered when a 5% frictional resistance is considered. Unlike the case without friction, the first mode is a mixed longitudinal and transverse mode, while the second and subsequent modes are in the transverse direction. Table 1 compares between the periods obtained by employing different bearing frictional resistance and elastic stiffness (K). The elastic stiffness is calculated from the shear modulus (G), plan area (A) and total elastomer thickness (t). Thus, $K=G\times A/t$. Clearly, the dynamic characteristics are not influenced by increasing the frictional resistance, while they are marginally affected by the elastic stiffness of the pad. The significant changes in dynamic characteristics reflect the pressing need to investigate the effect of bearing friction on the inelastic response of the bridge.

Response spectrum analysis is performed using the design response spectrum (AASHTO Standard Specifications 1995). Thirty-six modes of vibration are employed to reach a 90% mass participation in the two principle directions. The Complete Quadratic Combination (CQC) method, which accounts for the coupling between modes, is used to combine the modal forces and displacement. The demands imposed on the bridge from this analysis are summarized in Table 2. The results are similar to those used in the design, which lend extra weight to the analytical models developed in the current study and allows for comparisons between the design parameters obtained from SAP2000 elastic analysis and Zeus-NL inelastic pushover and response history procedures.

Table 1: Comparison between periods of vibration of different analytical modeling.

Period	**SAP2000 design conf.**[a] (sec.)	**Zeus-NL design conf.** [a]		**Zeus-NL as-built configuration**[b]					
				5% Friction *(stiffness = K)*		30% Friction *(stiffness = K)*		30% Friction *(stiffness = 6K)*	
		Period (sec.)	*Diff (%)*	*Period* (sec.)	*Diff (%)*	*Period* (sec.)	*Diff (%)*	*Period* (sec.)	*Diff (%)*
T1	1.518	1.422	6.3	0.796	47.6	0.796	47.6	0.764	49.7
T2	1.207	1.130	6.4	0.763	36.8	0.763	36.8	0.709	41.3
T3	0.802	0.786	2.0	0.709	11.6	0.709	11.6	0.659	17.8
T4	0.748	0.732	2.1	0.651	13.0	0.651	13.0	0.608	18.7
T5	0.748	0.699	6.6	0.609	18.6	0.609	18.6	0.594	20.6

[a]*: Design configuration: Friction is neglected and characteristics values of material strength are used*
[b]*: As-built configuration: Bearing friction and mean values of material strength are considered*
K: The elastic stiffness of the elastomeric pad.

Table 2: Seismic demands of the design configuration from response spectrum analysis.

Support	**Longitudinal Response**[a]		**Transverse Response**[a]	
	Shear (kN)	*Disp. (mm)*	*Shear (kN)*	*Disp. (mm)*
Pier No.1	3185	62	1721	17
Pier No.2	1472	62	2260	33
Pier No.3	1472	62	2811	42
Pier No.4	1130	63-82 *(for Unit 1 & 2)*	3350	50
Pier No.5	1148	81	3123	45
Pier No.6	1837	78	2415	35
Pier No.7	4057	74	2411	24
Pier No.8	1383	69	2015	20

Demands are at the pier base (forces) and at the pier top (displacements).
[a]*: Seismic load and measured demands are either in the longitudinal or transverse direction.*

Shortcomings of the design modeling assumptions are exemplified from the results of response spectrum analysis, particularly in the longitudinal direction. High base shear demands are attracted to Pier 1 and 7. Since these short piers are provided with pined bearings, they attract higher seismic demands due to their higher stiffness. Pier 8 does

not effectively participate in resisting the lateral forces due to neglecting the PTFE slider friction in the design modeling. The non-uniform distribution of displacement demands between Unit 1 and 2 is also clear since both units are uncoupled and vibrate independently.

CAPACITY ESTIMATES AND PRIORITIZING LIMIT STATES

Modern seismic design codes and guidelines (e.g. EC8 2004; FEMA 450 2003) adopt static pushover analysis as a design and assessment tool. The sequence of yielding and failure as well as the progress of the overall capacity curve of the structure are traced in the current study for both the design and the as-built configurations. This identifies potential structural deficiencies, enables estimation of the lateral capacity and provides insight into the limit state criteria required for response history analysis. To represent the distribution of inertia forces imposed on the bridge, lateral force profiles are calculated as a combination of load distributions obtained from eigenvalue analysis. A number of modes of vibration in the longitudinal and transverse directions are selected based on their mass participation to calculate the load patterns in the two principle directions. The gaps at the abutments and the expansion joints (refer to Figures 4) are not modeled in this incremental analysis to allow reaching the ultimate capacity and obtain complete capacity envelopes of the structure and its piers. Accordingly, the adopted target displacement corresponds to the drift collapse limit state.

Analysis of Individual Piers

The height of Piers 1, 7 and 8 is 50 feet, while it is 70 feet for other intermediate piers, as shown from Figure 3. Pushover analysis is thus carried out on each of the two pier configurations in the longitudinal and transverse directions to estimate their lateral capacity. In this analysis, the pier is free at top and the foundation is modeled as discussed earlier. The cross section at the base of the pier is 6.25×20 feet. This justifies the higher capacity in the transverse direction (400%) compared with the longitudinal one, as shown in Figure 8. Clearly, the stiffness and capacity of the shorter pier is higher than its counterpart. The increase in capacity when the mean material strength is used in analysis is about 9% compared with the case employing characteristic strengths.

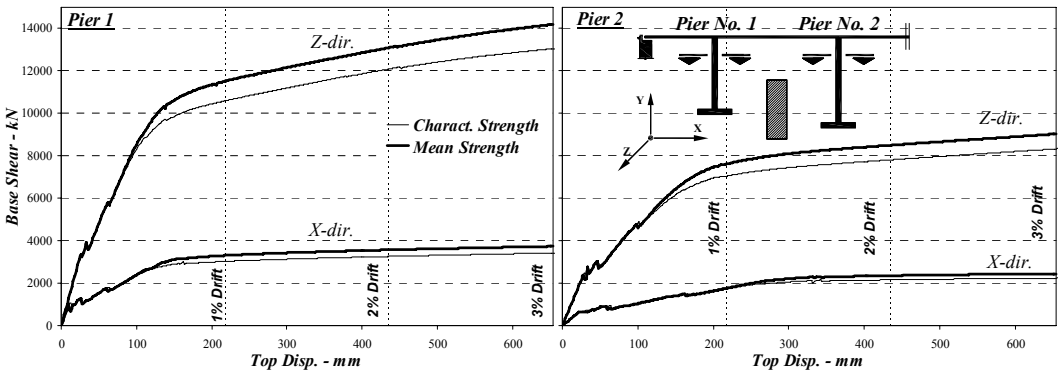

Figure 8. Capacity envelopes of Piers 1 and 2 in the longitudinal and transverse directions using characteristic and mean material strength.

Analysis of the Bridge in the Transverse Direction

Since the bridge is not symmetric, the analysis is carried out in both the positive and negative Z-direction. Figure 9 shows comparison of the sequence of plastic hinge formation and the capacity envelope of the design and the as-built configurations when applying the incremental load in the Z-direction. The idealized capacity envelope of the as-built bridge is also shown. The top displacement is the absolute value at the top of Pier 4, where the maximum drift is observed, while the base shear is the absolute total base shear of all piers. The drift limits (1, 2 and 3%) shown on the graph are based on the height of Piers 2 to 6, which govern the response of the bridge in the transverse direction. The following observations are worth mentioning:

- The increase in capacity of the as-built model compared with the design assumption is about 5%. For the design model, which disregards friction, the response is identical when applying the load in the positive and negative Z-direction. For the as-built configuration, the capacity in the positive Z-direction is slightly higher (2%). This is due to the contribution of the sliders frictional resistance of the curved unit.
- First indication of local yielding occurs at the base of Pier 4. This is attained at a total base shear higher than the design level. This is an indication that the transverse response will remain in the elastic range under the design earthquake.
- Global yielding is estimated from the idealized response of the as-built bridge at a drift of 1.3%. This is lower than the design assumption (1.5%), which has lower initial stiffness due to disregarding bearing friction. The

ultimate capacity is significantly higher than the design shear force. The observed overstrength (Ω_d = actual /design strength = 2.4) reflects the reliability of the bridge in this direction (Elnashai and Mwafy 2002).

- No degradation in lateral strength or sway mechanism are observed up to the drift collapse limit state. The pertinent performance indicators in this direction are therefore: (i) the segment collision at abutments; (ii) the drift (1.5% for yielding and 3.0% for collapse); and (iii) member criteria (local yielding and ultimate curvature). As a result of the curvature of the bridge, the longitudinal collision at abutments is the controlling collapse criterion even when applying the load in the transverse direction.

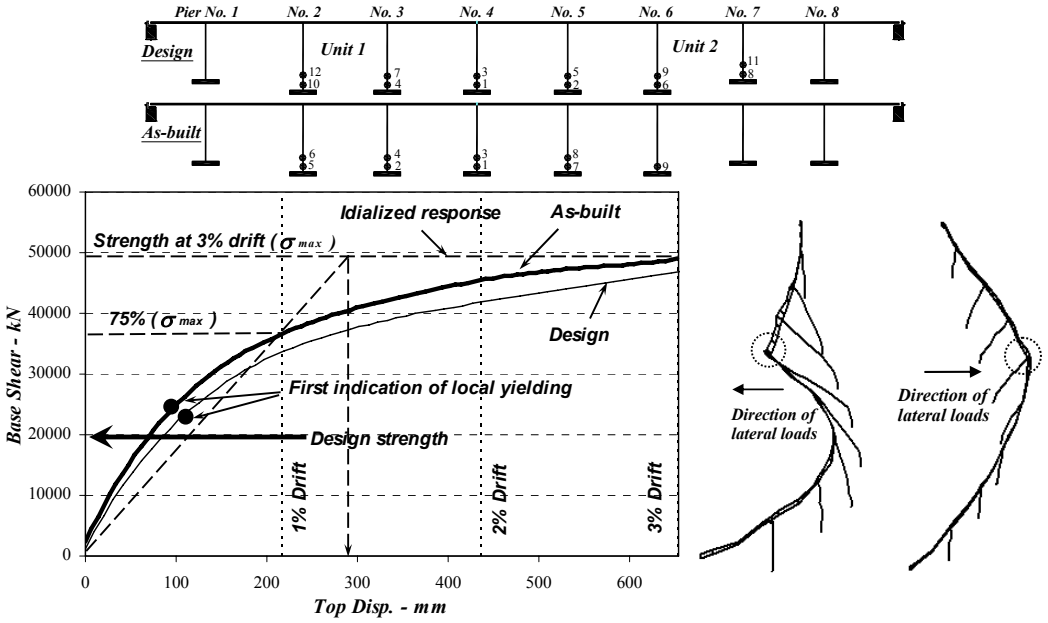

Figure 9. Mapping of sequence of plastic hinge formation and capacity envelope of the design and the as-built configurations in transverse direction.

Analysis of the Bridge in Longitudinal Direction

Longitudinal movement of the superstructure is controlled by the bearing friction, which follows the modeling approach explained earlier for the design assumption and the as-built configurations. Since the bridge in this direction consists of two units with distinct characteristics, the analysis is performed separately for each unit. For Unit 1, the incremental lateral load is applied in the negative X-direction, while it is in the positive X-direction for Unit 2. This is undertaken to avoid the collision between the two units, as indicated in Figure 10. Comparisons of

the sequence of plastic hinge formation and the capacity envelope of the design and the as-built configurations are shows in Figure 10. This is shown for the two units of the bridge. The capacity envelopes of individual piers obtained from analysis of the two units are depicted in Figure 11(a), while a comparison between capacity of the design assumption and the as-built bridge is depicted in Figure 11(b). The following observations are worthy of consideration:

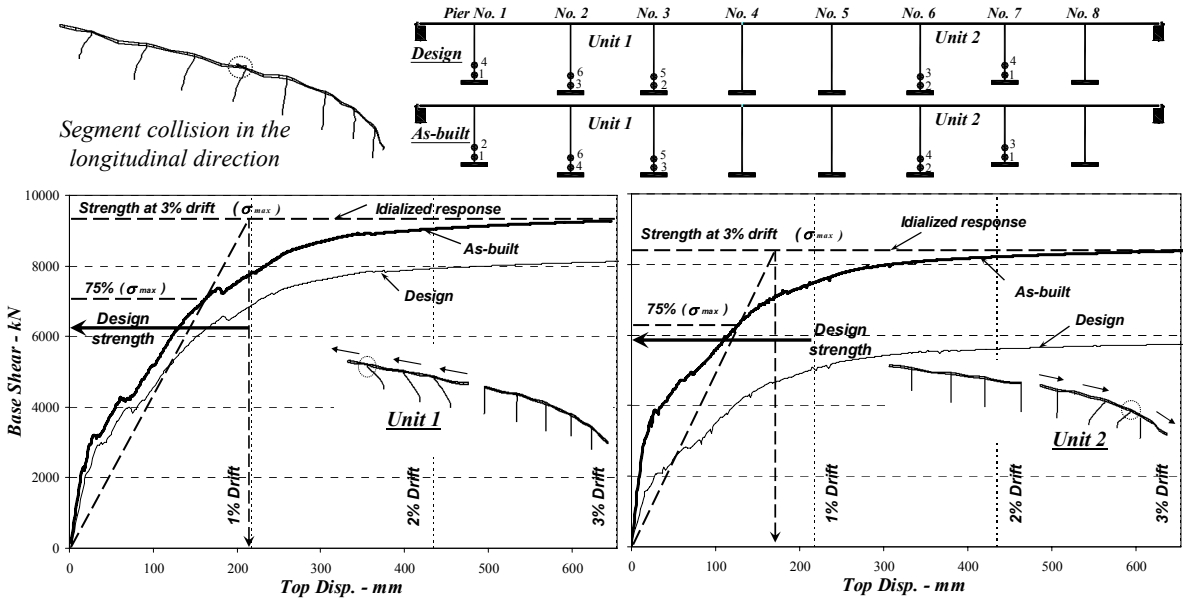

Figure 10. Mapping of sequence of plastic hinge formation and capacity envelope of the design and the as-built configurations in the longitudinal direction.

Unit 1:

- For the design configuration, the capacity envelopes of piers are comparable to those obtained from pushover analysis of individual piers. The ultimate capacity is slightly higher than the design force. The observed overstrength factor (Ω_d) is only 1.33.
- For the as-built configuration, the capacity envelopes of piers are higher than those obtained from pushover analysis of individual piers due to the contribution of bearing friction at Abutment A and at the expansion joint. The ultimate capacity of this unit is therefore higher than that for the design configuration by 15%, while the observed overstrength is 1.5.

- No degradation in lateral strength is observed up to a 3% drift. Global yielding is estimated from the idealized response at a 1.0% drift. It is also clear from Figure 11(a) that the potential sway mechanism of this unit, which involves formation of plastic hinges at the base of Piers 1 to 3, develops at a drift of 1.1%. These limit states are attained at higher deformations than the gap width at Abutments A (101.6 mm ~ 0.46%). Hence, the controlling limit state criterion of this unit is the collision at Abutments A.

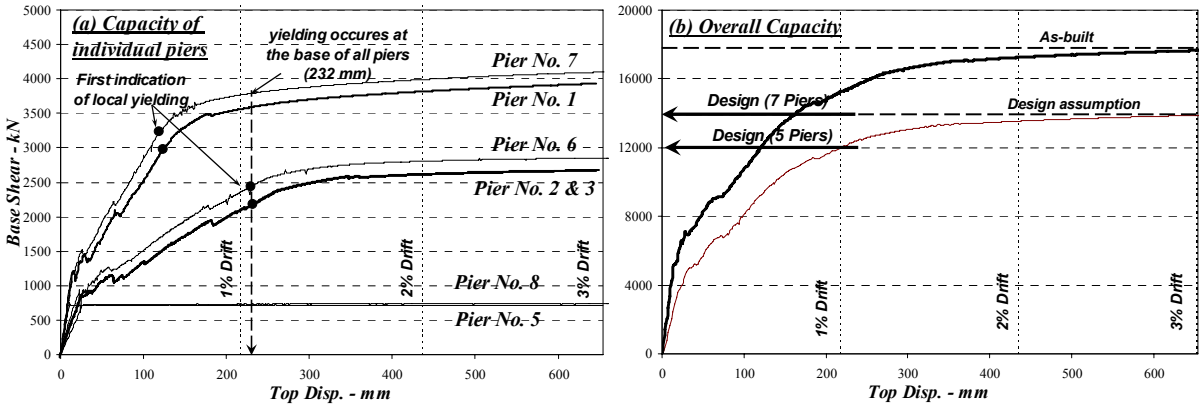

Figure 11. Response of the bridge in the longitudinal direction: (a) base shear-top displacement envelopes of individual piers of the as-built configuration; (b) capacity envelope of the design and the as-built bridge.

Unit 2:

- Since this curved unit is 40% longer than Unit 1, it has higher gravity loads and masses. For the design configuration, the lateral loads imposed on this unit, which is proportional with vertical loads, are only resisted by Piers 6 and 7. Hence, the lateral force resisting system is significantly less efficient than that of Unit 1.
- The design base shear of Pier 7 is slightly higher than its ultimate capacity. This is a common problem in bridges crossing steep-sided river valleys. Since the cross sections of the piers are identical, the shorter pier resists a higher level of inertia forces than the taller one. Although the actual capacity of Pier 7 is higher than that estimated for the design configuration since conservative material strengths are utilized, the capacity-to-design ratio is alarming.
- Unlike the design assumption, all piers of the as-built configuration participate in resisting lateral forces. Hence, the ultimate strength is 50% higher than the as-designed structure. The capacity envelopes of Piers 5 and 8, which participate in resisting lateral forces in this modeling, are equivalent to the frictional resistance of

the PTFE bearings. The capacity of Piers 6 and 7 is higher than that obtained from individual piers. Overstrength is 1.4, which represents an observable enhancement compared with the design configuration.

- No degradation in lateral strength is observed up to a 3% drift. It is also clear from Figure 11(a) that the sway mechanism, which involves formation of plastic hinges at the base of Piers 6 and 7, develops at a drift of 1.1%. Global yielding is estimated at a drift of 0.8%. These limit states are attained at higher deformations than the gap width at Abutments B. Hence, the limit state that controls the response of this unit is the collision at Abutment B.

Entire Bridge:

- The overall capacity increases by 30% as a result of the added resistance from the movable bearings at intermediate piers and at abutments.
- In the transverse direction, the pier stiffness is significantly higher than the longitudinal direction and all piers fully participate in resisting the lateral forces. Therefore, the lateral capacity is considerably higher than the longitudinal direction (240% and 180% for the design and the as-built configuration, respectively).
- The drift at local and global yielding is higher than the gap width at the two abutments. The controlled deformation at abutments prevents undesirable modes of failure since the response is in the elastic range. The collision at abutments is thus the governing performance criterion in the longitudinal direction.

CONCLUSIONS

A multi-span curved bridge was selected to investigate the significance of frequently-used design assumptions on seismic integrity of highway bridges. As opposed to undertaking extensive parametric studies where the parameters are varied not necessarily according to design specifications, this work focused in intricate detailing of one case of a realistic, office-designed and checked complex bridge. Refined three-dimensional modeling approaches were verified and employed to compare between the elastic and inelastic behavior of the design and the as-built configurations. The adopted methodology and results of the comprehensive analysis performed to estimate the dynamic characteristics, capacities and limit state criteria were presented. The following conclusions were drawn:

- The main modeling parameters affecting the dynamics characteristics were: bearing support modeling, material representation and superstructure idealization. The modes of vibration were significantly and fundamentally

different and the fundamental period decreased by 50% when the bearing frictional resistance was accounted for. Without friction the two units of the bridge vibrated independently in the longitudinal direction, while friction linked them together at the expansion joint. Due to the curvature of the bridge and the non-uniform distribution of stiffness and mass, higher modes notably contributed to seismic response.

- In the transverse direction, the response was less affected by friction due to restraining the PTFE sliders by girder stops. The capacity increase of the as-built model was 5%. Overstrength was 2.4 and first yielding was attained at a base shear higher than the design value, confirming the high margin of safety and the anticipated elastic response under the design earthquake. Pushover analysis confirmed that the collision at abutments was the controlling performance criterion even when seismic loads were applied in the transverse direction of the curved bridge.
- To avoid collision between the two units of the bridge, pushover analysis was performed independently for Unit 1 and 2 by applying the incremental load in two opposite directions. For Unit 1, overstrength of the as-built configuration increased from 1.33 to 1.5. Global yielding and the sway mechanism were estimated at a drift higher than the gap width at the abutments. The controlling limit state criterion of Unit 1 was therefore the collision at Abutments A.
- For the design configuration, Unit 2 was less efficient in the longitudinal direction than Unit 1 due to excluding the PTFE piers from resisting lateral loads. As the bridge crosses a steep-sided river valley, response of a short stiff pier was critical due to the high attracted inertia forces. Overstrength of Unit 2 was almost unity, confirming its high vulnerability. For the as-built configuration, all piers participated in resisting lateral forces. Hence, the capacity was 50% higher than the as-designed structure. For both configurations, global yielding and the sway mechanism developed at a drift akin to that observed for Unit 1. Hence, the controlling limit state for Unit 2 is the collision at Abutments B. Pushover analysis confirmed that the superstructure-abutment zones controlled the response in the two principle directions of the curved bridge.

The study emphasizes the significance of pushover analysis procedures in verification of analytical modeling, identifying potential structural deficiencies, estimating capacity and providing insight into the limit states of complex bridges. The major difference between modeling the bridge as-designed and as-built was the inclusion of bearing friction. The dynamic characteristics changed fundamentally and the capacity increased significantly when

friction was included, using a conservative friction coefficient. The latter change led to an adverse impact on seismic demands due to the significant reduction in the periods of vibration. Conventional design assumptions, such as zero friction on intermediate piers, may therefore lead to non-conservative designs. This is confirmed from comparisons of capacities and demands predicted from response history analysis.

ACKNOWLEDGMENTS

This study was funded by the US Federal Highway Administration (FHWA) through the Mid-America Earthquake Center (MAE), University of Illinois at Urbana-Champaign, USA. The MAE Center is an Engineering Research Center funded by the National Science Foundation under cooperative agreement reference EEC 97-01785.

REFERENCES

1. AASHTO Standard Specifications (1995). *Standard specifications for highway bridges*, 15th Ed., American Association of State Highway and Transportation Officials, Washington, D.C.
2. Antoniou, S., and Pinho, R. (2004). "Advantages and limitations of adaptive and non-adaptive force-based pushover procedures." *J. of Earthquake Engineering*, 8(4), 497-522.
3. Bondonet, G., and Filiatrault, A. (1997). "Frictional Response of PTFE Sliding Bearings at High Frequencies." *J. of Bridge Engineering*, 2(4), pp. 139-148.
4. Caltrans (2004). *Caltrans Seismic Design Criteria*. California Department of Transportation, Sacramento, CA.
5. Choi, E., DesRoches, R., and Nielson B. (2004). "Seismic fragility of typical bridges in moderate seismic zones." *Eng. Structures*, 26, 187–199.
6. Constantinou, M. C., Mokha, A., and Reinhorn, A. M. (1990). "Teflon bearings in base isolation II: Modeling." *J. of Structural Engineering*, 116(2), 455–474.
7. CSI (2003). *SAP2000 – Structural analysis program*, Computers and Structures, Inc., Berkeley, California.
8. EC8 (2004). Eurocode 8: *Design of structures for earthquake resistance - Part 1: General rules, seismic actions and rules for buildings, and Part 2: Bridges*, CEN, European Committee for Standardization, Brussels.
9. Elnashai, A.S. (2001). "Advanced inelastic static (pushover) analysis for earthquake applications." *J. of Structural Engineering and Mechanics*, 12(1), 51-69.
10. Elnashai, A.S. (2002). "Do we really need inelastic dynamic analysis?." *J. of Earthquake Engineering*, 6(Special Issue 1), 123-130.
11. Elnashai, A.S., and Mwafy, A.M. (2002). "Overstrength and force reduction factors of multistorey reinforced-concrete buildings." *The Structural Design of Tall Buildings*, 11(5), 329–351.
12. Elnashai, A.S., Papanikolaou, V., and Lee, D. (2004). *Zeus-NL - a system for inelastic analysis of structures*, User Manual, Mid-America Earthquake Center, Civil and Environmental Engineering Department, Univ. of Illinois at Urbana-Champaign, Urbana, IL.
13. FEMA (2003). *NEHRP recommended provisions for seismic regulations for new buildings and other structures (FEMA 450)*, Federal Emergency Management Agency, Washington, D.C.

14. Izzuddin, B.A., and Elnashai, A.S. (1989). *ADAPTIC – A program for adaptive large displacement elastoplastic dynamic analysis of steel, concrete and composite frames*, ESEE Research Report No. 89/7, Imperial College, Univ. of London, UK.
15. FHWA (1996). *Seismic design of bridges – Design example No. 5 – Nine-span viaduct steel girder bridge*, US Department of Transportation, Publication No. FHWA-SA-97-010.
16. Jeong, S.-H., and Elnashai, A.S. (2005). "Analytical assessment of an irregular RC frame for full-scale 3d pseudo-dynamic testing - Part I: Analytical model verification." *J. of Earthquake Engineering*, 9(1), 95-128.
17. Lu, Z., Ge, H., and Usami, T. (2004). "Applicability of pushover analysis-based seismic performance evaluation procedure for steel arch bridges." *Engineering structures*, 26(13), 1957–1977.
18. Maroney, B.H. (1995). *Large scale bridge abutment tests to determine stiffness and ultimate strength under seismic loading*, PhD Thesis, University of California, Davis.
19. Muthukumar, S., and DesRoches, R. (2006). "A Hertz contact model with non-linear damping for pounding simulation," *Earthquake Eng. Struct. Dyn.*, 35(7), 811-828.
20. Mwafy, A.M., Elnashai, A.S., and Yen, W-H. (2006-a). "Implications of design assumptions on capacity estimates and demand predictions of multi-span curved bridges", ASCE Journal of Bridge Engineering, In Press.
21. Mwafy, A.M., Elnashai, A.S., Sigbjörnsson, R., and Salama, A. (2006-b). "Significance of severe distant and moderate close earthquakes on design and behavior of tall buildings." *The Structural Design of Tall and Special Buildings*, Vol. 15(4), 391-416.
22. Mwafy, A.M., and Elnashai, A.S. (2002). "Calibration of force reduction factors of RC buildings." *J. of Earthquake Engineering*, 6(2), 239-273.
23. Mwafy, A.M., and Elnashai, A.S. (2001). "Static pushover versus dynamic collapse analysis of RC buildings." *Engineering Structures*, 23(5), 407-424.
24. Priestley, M.J.N., Seible, F., and Calvi, G.M. (1996). *Seismic design and retrofit of bridges*, Wiley, New York.
25. Rossetto T., and Elnashai, A.S. (2005). "A new analytical procedure for the derivation of displacement-based vulnerability curves for populations of RC structures." *Engineering Structures*, 27(3), 397–409.
26. USGS (2002). "Seismic hazard maps for the conterminous U.S. for 2002." U.S. Geological Survey Earthquake Hazards Program, <http://earthquake.usgs.gov> (Jan. 31, 06).
27. Zheng, Y., Usami, T., and Ge, H. (2003). "Seismic response predictions of multi-span steel bridges through pushover analysis." *Earthquake Engineering and Structural Dynamics*, 32(8), 1259–1274.

Assessment of Seismic Integrity of Multi-Span Curved Bridges in Mid-America

Part II: Comparative Assessment of the Designed and As-Built Simulations of Complex Bridges Subjected to Increasing Earthquake Intensities

by

A.M. Mwafy and A.S. Elnashai

Mid-America Earthquake Center
Civil and Environmental Engineering Department
University of Illinois at Urbana-Champaign, IL, USA

April 2007

This research is supported by the Mid-America Earthquake Center
under National Science Foundation Grant EEC-9701785

TABLE OF CONTENTS

SUMMARY

The significance of simplified design assumptions on seismic integrity of highway bridges is investigated in this study by comparisons of the 'as-built' and the 'as-designed' seismic response of a nine-span curved bridge at the design and twice the design earthquake intensity. The prototype bridge was selected from the inventory of the Federal Highway Administration (FHWA) concept designs to represent a US typical design of multi-span curved bridges with superstructure-pier bearings. Extensive inelastic response history analyses are performed using verified three-dimensional fiber idealizations to predict the capacity-to-demand ratios of the bridge components in the longitudinal and transverse directions. A diverse set of artificially generated ground motions characterizing two distinct soil profiles and three earthquake scenarios with increasing severity is employed. Comparisons of seismic demands with available capacities show that advanced analysis is versatile and sensitivity studies, as opposite to approximates, are essential for complex bridges. Seemingly conservative design assumptions, such as ignoring friction at the bearings, may lead to erroneous and potentially non-conservative response expectation. Changes in dynamic characteristics may increase seismic loads, leading to redistribution and magnification of demands. Conservative modeling of bearing friction maintains a level of coupling between the superstructure and piers provided with PTFE sliders even at high levels of ground motion. The recommendations given are of assistance to design engineers seeking to achieve realistic predictions of seismic behavior and thus contribute to uncertainty reduction in the ensuing design.

INTRODUCTION

Research carried out during the past two decades has led to significant changes in seismic design provisions of bridges. The introduction of the AASHTO Load and Resistance Factor Design (LRFD) Specifications (2005) is aimed at providing more uniform safety for different types of bridge system. Several state departments of transportation have fully or partially implemented LRFD specifications, while others are working with the Federal Highway Administration (FHWA) to develop implementation plans. These revisions in design specifications draw attention to the need for seismic assessment of complex highway bridges designed to preceding provisions to determine the level of risk associated with loss of serviceability or possible damage. This is particularly important in the light of recent increase in seismic design criteria for several regions in the US such as the central Mississippi Valley (USGS 2002).

Structural analysis of multi-span bridges for earthquake design often employs simplifying assumptions such as the uncoupling between superstructure and piers provided with PTFE/stainless steel sliders by assuming zero bearing friction. While the infinite frictionless bearings cannot be achieved in practice, such assumption is justified in many instances. There are little studies in the literature addressed the significance of different simplifying modeling assumptions, particularly for multi-span curved bridges. Part I of this study have presented a methodology to investigate impact of conventional design assumptions on dynamic characteristics and capacity estimates of multi-span complex bridges by comparisons with 'as-built' simulations. The as-built behavior was predicted by realistically modeling bridge bearings and their frictional resistance, structural gaps and materials. Eigenvalue, response spectrum, inelastic pushover analyses were undertaken for a nine-span curved bridge. The study emphasized the significance of pushover analysis in verification of analytical modeling, identifying potential structural deficiencies, estimation of capacity and prioritizing limit state criteria. The dynamic characteristics conceptually change and the lateral capacity increases significantly when considering bearing friction. The significant reduction in period suggested an adverse impact on demands due to magnification of seismic loads.

This Report addresses the significance of the coupling between the superstructure and piers provided with PTFE sliders on the inelastic seismic integrity of complex bridges, which comprises the second phase of this study (Mwafy et al., 2006). Seismic assessment of multi-span curved bridges designed to the AASHTO Standard Specifications (1995) under increased level of ground motions is also investigated. A number of parameters are studied to tune the analytical models for inelastic response history analysis, including direction of seismic loads, damping level and integration schemes. Extensive inelastic response history analysis are then undertaken to predict the seismic demands for the as-designed and the as-built configurations. Capacity-demand predictions of the nine-span bridge on both the member and the structure levels are finally compared.

INGREDIENTS OF THE ASSESSMENT STUDY

Structural Modeling and Performance Indicators

The plan and elevation of the investigated bridge are shown in Figure 1. Detailed description of the 1488 feet nine-span curved bridge is provided elsewhere in Part I of this study (FHWA 1996). Two modeling approaches are considered in the current study to investigate the significance of conventional design assumptions on capacity-demand predictions of complex bridges. These are the 'design assumption' and the 'as-built' behavior. The latter modeling realistically accounts for bridge bearings and their frictional resistance, structural gaps and material response. The refined three-dimensional modeling approaches adopted to idealize the entire bridge and its foundation for elastic and inelastic analysis were described and verified in Part I of this study and by Mwafy et al. (2006). Inelastic response history analysis is carried out herein using the Mid-America Earthquake Center inelastic analysis program Zeus-NL. The program has been extensively used in seismic design and assessment of buildings and bridges and has been verified against full scale tests from Europe and the US. Further information about the program and its comprehensive libraries and efficient nonlinear solution procedure is mentioned elsewhere (Elnashai et al. 2004).

The adopted yield and collapse performance indicators were also discussed in Part I of the present study and by Mwafy et al. (2006). Pushover analysis was employed to investigate and prioritize the selected set of limit state criteria for response history analysis. The deformation restrictions at abutments prevented formation of undesirable

modes of failure such as the core concrete crushing or the excessive drift and hinging mechanism. Hence, the collision at superstructure-abutment zones controlled the response in the two principle directions due to the curvature of the bridge. Nevertheless, the seismic response in response history analysis is monitored using the entire set of limit state criteria. This is undertaken to verify the conclusions obtained from pushover analysis due to the structural system complexity and anticipated higher modes effect.

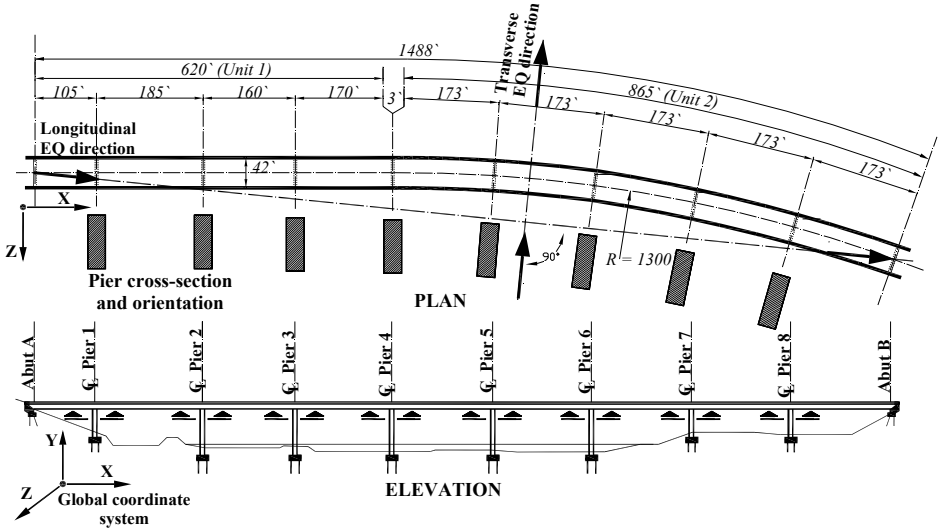

Figure 1. Plan and elevation of the investigated bridge showing the difference between local and global coordinate systems.

Input Ground Motions

A set of artificially-generated input ground motions was carefully selected for this assessment study to represent typical earthquake scenarios in Mid-America (Rix et al. 2004). Table 1 shows characteristics of these accelerograms for the following earthquake scenarios:

1. M=7.5 at Blytheville, AR, with a focal depth of 10 km
2. M=6.5 at Marked Tree, AR, with a focal depth of 10 km
3. M=5.5 at Memphis, TN, with a focal depth of 20 km

The synthetic records were generated for two different soil profiles: Lowlands and Uplands. An 84% amplification factor was used for generating ten time histories for each of the three earthquake scenarios. Due to the similarity between these records, a single accelerogram was selected from each soil-earthquake scenario group. Hence, six

records were used in response history analysis. These are Lowland1, Lowland2, Lowland3, Upland1, Upland2 and Upland3.

Table 1: Synthetically generated input ground motions.

	Soil Profile	*Peak Ground Motion Parameter*	*Scenario 1: M = 7.5 at Blytheville, AR*	*Scenario 2: M = 6.5 at Marked Tree, AR*	*Scenario 3: M = 5.5 at Memphis, TN*	*No. of Records*
1	**Lowlands**	**PGA (g)**	**0.1427**	**0.0632**	**0.0958**	3
		PGV (m/s)	0.152	0.0576	0.0665	
		PGD (m)	0.0606	0.0202	0.0138	
2	**Uplands**	**PGA (g)**	**0.1407**	**0.0676**	**0.103**	3
		PGV (m/s)	0.129	0.0516	0.0609	
		PGD (m)	0.0537	0.0178	0.0118	

Figure 2 depicts the acceleration time histories of the selected records and compares their elastic spectra with the design one (AASHTO Standard Specifications 1995). It is clear that the spectra of the records generated for Scenario 1 (M=7.5 at Blytheville, AR) reasonably match the design spectrum. They are slightly higher in the period range below 1.0 sec, particularly Lowland1, and lower than the design spectrum in the long period range. The latter record is likely to produce the highest demands due to its high amplification at 1.7 sec, which may coincide with the fundamental cracked period of the design configuration in the longitudinal direction ($T_{1\ uncracked} = 1.42$). The PGAs of Scenario 1 records are also akin to the design (0.15g), as shown from Table 1. Therefore, Scenario 1 records are used for assessment of the design acceptability, while records generated for Scenarios 2 and 3 are used to check the serviceability limit states.

Furthermore, in view of recent changes in the seismic hazard of several medium seismicity regions in the US (USGS 2002), vulnerability of the case study bridge to higher levels of ground motions than the design earthquake is investigated in this study. Assessment of the structure under the most credible earthquake is performed by scaling the records generated for Scenario 1 to twice the design earthquake. This conservative assumption implies that the seismicity of the site is increased by 100%.

Several approaches for scaling input ground motions have been suggested in the literature. A procedure based on the velocity spectrum intensity (Housner, 1952) and employs the inelastic period of the structure was adopted by Elnashai and Mwafy (2002) and Mwafy and Elnashai (2001). The natural records are scaled in this approach to possess equal velocity spectrum intensity in the period range of the structure, whilst the design spectrum is taken as a reference. This approach is significant when employing natural ground motions in the analysis. The more simplified approach of scaling the accelerograms using PGAs is adopted in the present study since the synthetic records of scenario 1 have spectrum intensities comparable to the design spectrum. The adopted set of accelerograms and PGAs thus ensure that the investigated structure is analyzed under input ground motions representing a wide range of possible seismic events at the site.

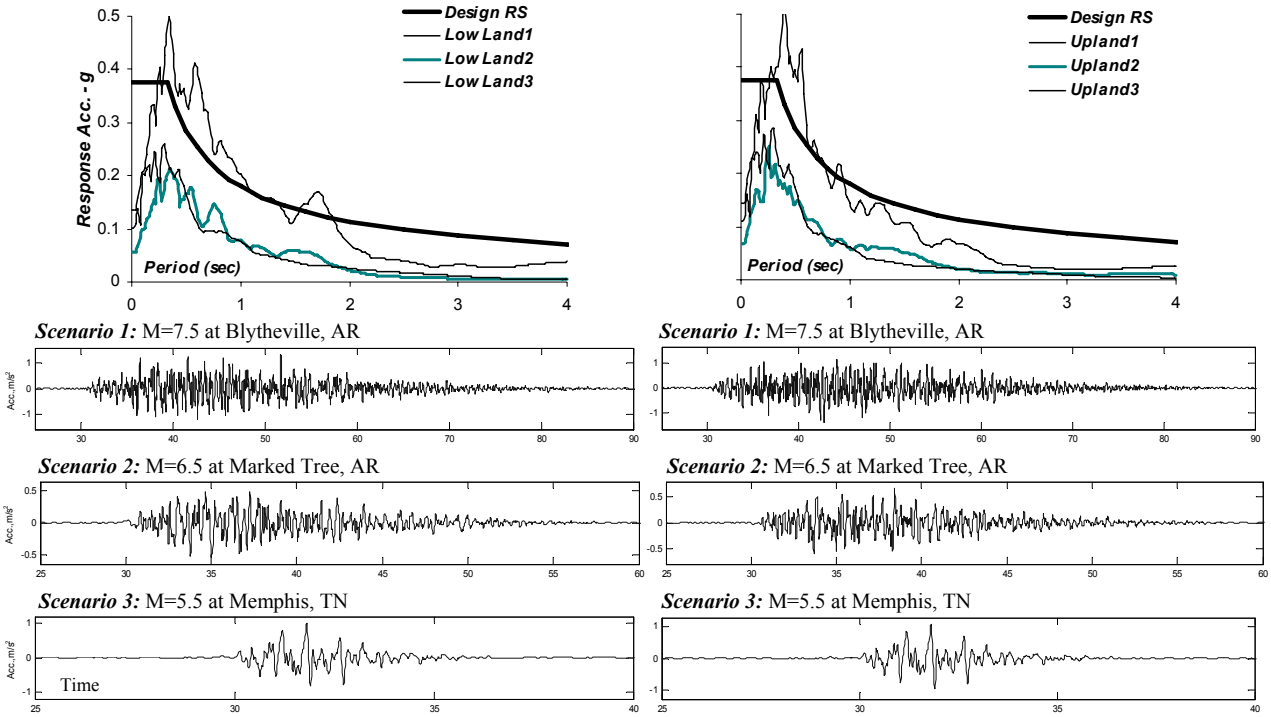

Figure 2. Comparisons between the selected earthquake scenarios and the design spectrum.

SELECTION OF DYNAMIC ANALYSIS PARAMETERS

Before executing the inelastic response history analysis, a number of parameters were investigated to tune the analytical models for this demanding analysis. Earthquake loads in the design phase were applied in the longitudinal

direction along a straight line connecting the two base nodes at the end abutments. In the transverse direction, loads were applied at a 90 degree to the longitudinal direction. As a result of the structure curvature, these directions are inclined at 11° from the global X and Z axes, as shown from Figure 1. SAP2000 allows employing user-defined local axes for loads, while the global coordinate system should be used in the inelastic analysis performed using Zeus-NL. Response spectrum and elastic response history analyses were therefore undertaken to investigate the significant of this inclination on the seismic demand predictions. Results obtained from applying the seismic loads in both the local and global coordinate systems confirmed the insignificance of this minor inclination and the applicability of using the global coordinate system in analysis. The analysis also emphasized the importance of employing a refined time step in response history analysis performed using the selected set of synthetic accelerograms. Thus, the analysis carried out using Zeus-NL employs the global coordinate system and a refined time step (0.01 – 0.02 sec).

Damping is modeled in Zeus-NL using Rayleigh damping elements. The mass- and stiffness-proportional parameters are calculated based on the predominant periods of the structure (Chopra 2000). Since the hysteretic damping due to inelastic energy absorption is already accounted for in the inelastic analysis, two levels of Rayleigh damping ratios are investigated; 1% and 2%. Table 2 shows comparison between results of elastic analysis with a 5% damping ratio and Zeus-NL inelastic response history analysis performed using different Rayleigh damping levels (0, 1 and 2%). An elastic response is anticipated under the design earthquake due to the high overstrength observed in the transverse direction (Mwafy et al. 2006). Therefore, it is anticipated to obtain comparable demands from inelastic analysis compared with those from elastic analysis. It is observed that the 2% Rayleigh damping ratio results in improved predictions of deformation and base shear demands, while those at the 1% damping are almost twice the elastic analysis results. It was decided to maintain the Rayleigh damping in inelastic analysis at the 2% level due to the high inelasticity expected in the longitudinal direction of the bridge (Mwafy et al. 2006).

The integration of equations of motion may be carried out in Zeus-NL by means of two different algorithms; Newmark or Hilber-Hughes-Taylor integration algorithm (Broderick et al. 1994). The HHT algorithm requires an additional parameter to control the level of numerical dissipation. Comparisons between results of the two schemes confirmed the similarity between their results at the design earthquake. As confirmed from the study of Broderick et

al. (1994), the HHT algorithm is more beneficial under high input ground motions since it can reduce the very high short-duration peaks in the solution. Therefore, to increase both the accuracy and the numerical stability of the analysis, the HHT scheme is employed in subsequent response history analysis.

Table 2. Comparison between elastic and inelastic demands at different damping levels (transverse direction).

Support	Elastic Analysis (5% Damping)		ZeusNL Inelastic Response History Analysis					
			0.0% Rayleigh Damping		1% Rayleigh Damping		2% Rayleigh Damping	
	Disp. (mm)	*Shear (kN)*	*Disp. (mm)*	*Shear (kN)*	*Disp. (mm)*	*Shear (kN)*	*Disp. (mm)*	*Shear (kN)*
Abutment A	10		32		17		14	
Pier No.1	17	1721	33	5601	17	4363	14	3874
Pier No.2	33	2260	70	4404	61	4119	54	3898
Pier No.3	42	2811	104	6430	74	4800	65	4572
Pier No.4	50	3350	147	7645	103	6375	75	5061
Pier No.5	45	3123	94	5742	71	4687	59	4168
Pier No.6	35	2415	87	5475	73	4507	64	4317
Pier No.7	24	2411	50	5144	34	3762	34	3322
Pier No.8	20	2015	64	4989	49	3303	41	3794
Abutment B	11		70		60		48	

Demands are at the pier base (shear) and at the pier top (displacements).

DEMAND PREDICTIONS AT THE DESIGN EARTHQUAKE

Response in Transverse Direction

Table 3 shows comparisons between the displacement and base shear demands of the design and the as-built configurations obtained from inelastic response history analysis using the selected set of ground motions. Figure 3 depicts a sample comparison between the maximum displacement time-histories at top of piers and abutments of the two modeling approaches investigated in this study.

The highest demands are generated from Lowland1 at Pier 4. The maximum displacement demands are higher by 50% than those obtained from response spectrum analysis using the design spectrum. This was expected since Lowland1 is higher than the design spectrum in the period range below 1.0 sec, as shown from Figure 2. It is noteworthy that the maximum total base shear demands shown in Table 3 are from summation of the response time-histories not from summation of the peak values.

The predominant cracked period in the transverse direction is 0.88 and 0.85 second for the design and the as-built models, respectively. These are estimated from Fourier analysis of the top acceleration response of Pier 4, as shown from Figure 4. The period of the structure in this direction is marginally influenced by the bearing friction, which is expected to be more pronounced in the longitudinal direction. The maximum demands of the as-built bridge are therefore akin to those of the design configuration. Nevertheless, comparison of the displacement time histories shown in Figure 3 confirms the significant change in response of the curved unit of the bridge (Piers 5-8 and Abutment B). Clearly, the significance of the bearing friction increases with the inclination of the local coordinate system. Hence, it is more pronounced on Abutment B compared with Pier 5, while it has no effect on the straight unit (Abutment A and Piers 1-3).

Table 3. Inelastic demands of the design and the as-built configurations in the transverse direction (*kN - mm*).

	Location	***Design***		***Lowland1***		***Lowland2***		***Lowland3***		***Upland1***		***Upland2***		***Upland3***	
		Disp.	*Shear*	*Disp.*	*Shear*	*Disp.*	*Shear*	*Disp.*	*Shear*	*Disp.*	*Shear*	*Disp.*	*Shear*	*Disp.*	*Shear*
Design	Abutment A	10		14		7		8		19		9		9	
	Top of Pier 1	17	1721	14	3874	7	1820	5	1300	19	4105	5	1387	5	1314
	Top of Pier 2	33	2260	54	3898	21	2469	13	1605	50	3997	16	2006	12	1462
	Top of Pier 3	42	2811	65	4572	28	2863	17	2145	44	3462	17	2172	16	1957
	Top of Pier 4	50	3350	75	5061	48	4275	26	2740	75	4947	31	3300	20	2541
	Top of Pier 5	45	3123	59	4168	39	3412	18	2297	48	3848	21	2717	17	2043
	Top of Pier 6	35	2415	64	4317	26	3044	15	1701	42	3544	20	2169	14	1533
	Top of Pier 7	24	2411	34	3322	10	3893	6	1332	23	3858	11	1742	6	1299
	Top of Pier 8	20	2015	41	3794	11	1887	9	1263	23	3115	12	2017	8	1251
	Abutment A	11		48		15		14		24		19		13	
	Total shear / Max disp.	**50**	**20106**	**75**	**25556**	**48**	**17532**	**26**	**11294**	**75**	**19412**	**31**	**13340**	**20**	**10234**
As-built	Abutment A			15		6		9		21		5		9	
	Top of Pier 1			19	4242	6	1729	5	1216	24	4337	5	1254	4	1153
	Top of Pier 2			53	3939	19	4084	12	2557	52	6341	11	2376	11	2190
	Top of Pier 3			59	4283	26	3607	17	2215	47	3601	15	1920	14	1838
	Top of Pier 4			78	5309	48	3702	26	3387	75	5198	22	3063	18	2395
	Top of Pier 5			54	4134	33	3702	17	2089	42	3885	16	2052	15	1824
	Top of Pier 6			53	4213	20	2329	12	1470	45	3625	12	1449	10	1267
	Top of Pier 7			19	3896	10	1989	5	1222	25	4075	6	1292	5	1091
	Top of Pier 8			24	4062	9	2314	6	1264	21	3478	6	1556	5	1198
	Abutment A			29		13		10		24		11		9	
	Total shear / Max disp.			**78**	**22140**	**48**	**16570**	**26**	**11239**	**75**	**22394**	**22**	**10824**	**18**	**9673**

Demands are at the pier base (shear) and at the pier top (displacements).

Comparisons of the relative displacement in the longitudinal direction at the abutments and the expansion joint for the design and the as-built configuration are depicted in Figure 5. Although seismic loads are applied in the transverse direction, the longitudinal response is significantly affected by the bearing modeling approach. For the design configuration, zero deformation demands are observed at Abutment A since Unit 1 of the bridge is straight and the seismic action is applied in the transverse direction. As a result of the curvature of Unit 2, the maximum displacement demand at the expansion joint and at Abutment B is 73 and 55 mm, respectively. When the bearing frictional resistance is considered, the two units of the bridge are coupled and the displacement demands are favorably redistributed between the expansion joint and the two abutment gaps, as shown from Figure 5(b). It is clear that a higher margin of safety, defined as the demand to the capacity (gap width), is achieved when considering the bearing friction.

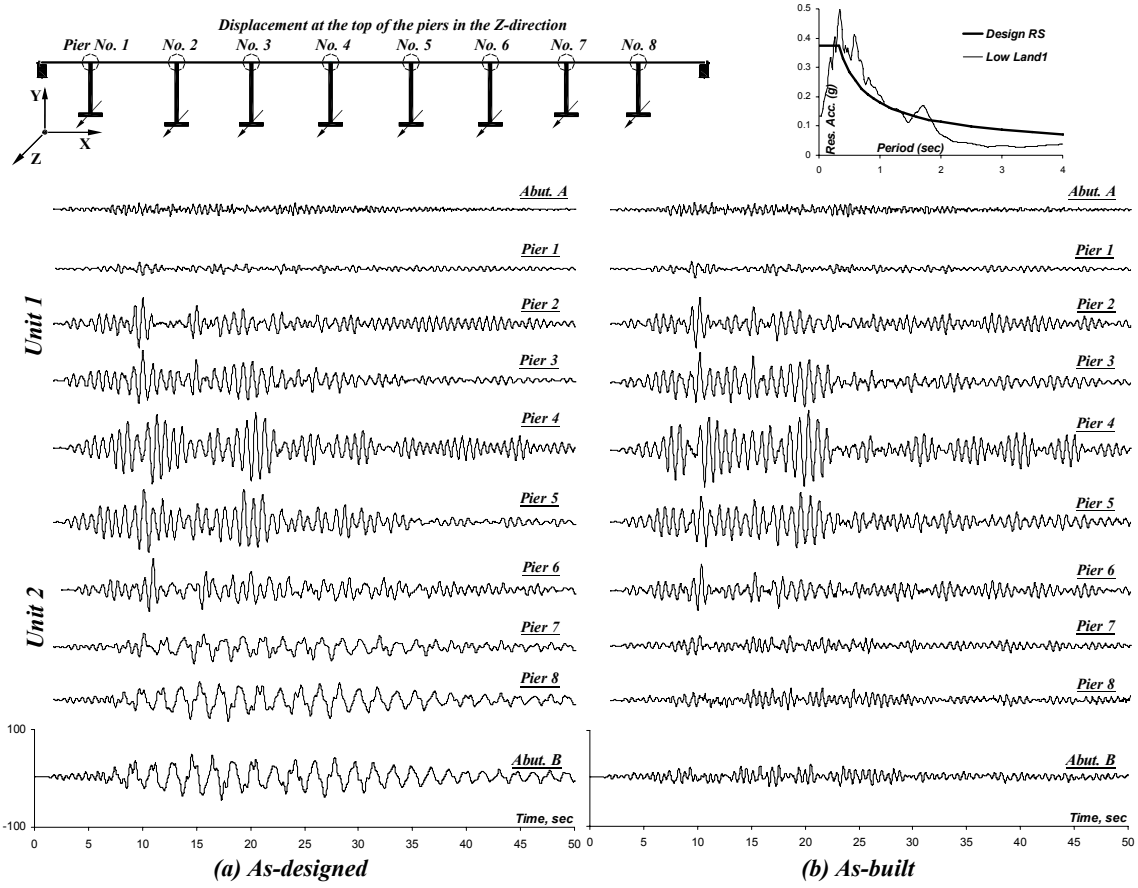

Figure 3. Comparison of displacement histories in the transverse direction at the design earthquake (Lowland1).

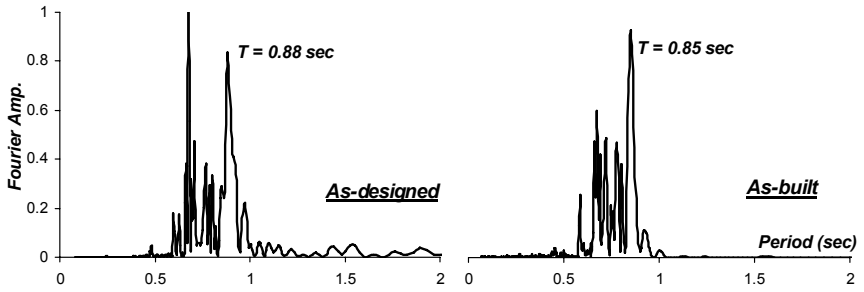

Figure 4. Fourier spectra of the acceleration response at top of Pier 4 (Lowland1).

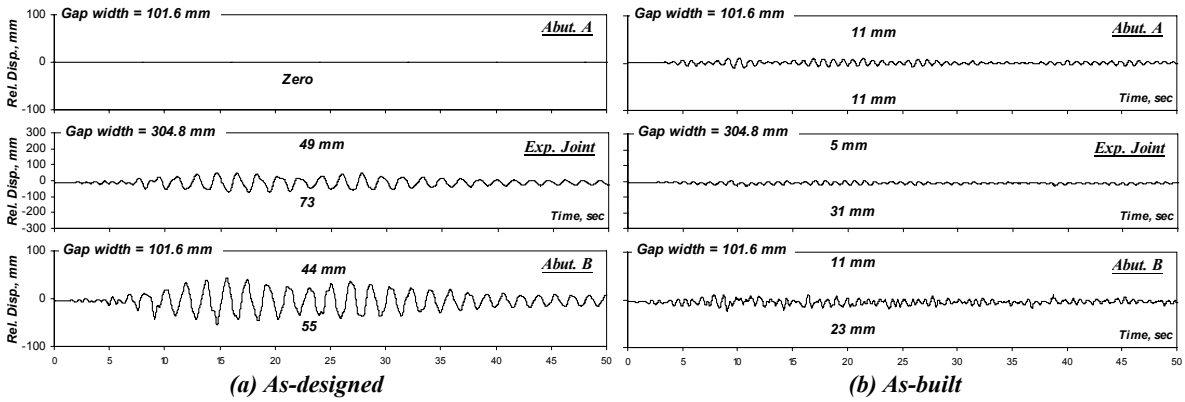

Figure 5. Comparison of relative displacement response in the longitudinal direction at the abutments and the expansion joint (load in transverse direction at the design EQ).

The elongation in period at the design earthquake is about 10% for the two analytical models investigated. This reflects a minor concrete cracking and a response within the elastic range. No yielding is observed under the effect of the six records employed here, confirming the high margin of safety. A comparison between the capacity and maximum base shear demand of the design assumption and the as-built bridge at the design and twice the design earthquake is shown in Figure 6. The capacities are estimated from inelastic pushover analysis of the entire bridge (Mwafy et al. 2006), while the demands are conservatively estimated from Lowland1, which produces the highest response. It is clear that maximum global demand under the design earthquake is well below the minimum supply and the response of both the design and the as-built configuration is within the elastic range.

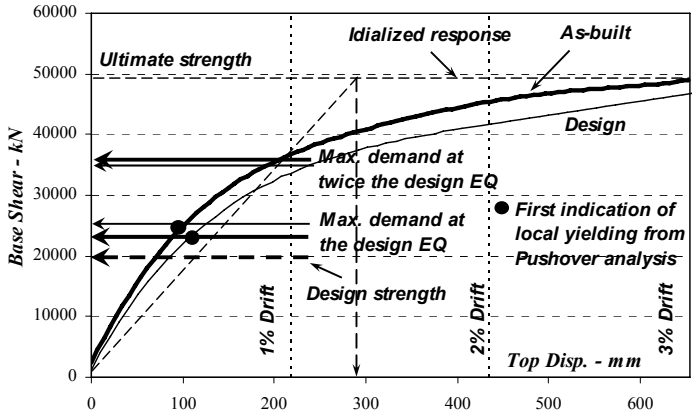

Figure 6. Capacity versus design and demand in the transverse direction (design and twice the design EQ).

Response in Longitudinal Direction

A summary of the maximum relative displacement and base shear demands from the selected set of ground motions is shown in Table 4. Figure 7 depicts comparison between the maximum displacement time-histories of the design and the as-built configurations obtained from Lowland1, which produces the maximum displacement and base shear demands. For the design configuration, the displacement demands from this record are higher than those used in design by about 75% and 25% for Unit 1 and 2, respectively. The displacement demands from other earthquake scenarios are lower than the design values. Base shear demands from the six records used are lower than the design base shear, particularly for Pier 1 and 7 which governed the design.

On the other hand, the displacement demands of the as-built configuration generally decrease due to the beneficial effect of bearing friction. In contrast, seismic loads significantly amplify as a result of the considerable reduction in period. Hence, the total base shear demands observed from the earthquake scenarios employed herein are significantly higher (up to 70%) than those from the design assumption. The maximum shear demand of a number of piers is higher by up to 110% than the design force. Owing to the high design overstrength, no crushing in concrete is observed. Nevertheless, this significant increase in seismic base shear is a clear indication that neglecting the bearing friction in the design is non-conservative.

Table 4. Inelastic demands of the design and the as-built configurations in the longitudinal direction (*kN - mm*).

	Location	***Design***		***Lowland1***		***Lowland2***		***Lowland3***		***Upland1***		***Upland2***		***Upland3***	
		Disp.	*Shear*	*Disp.*	*Shear*	*Disp.*	*Shear*	*Disp.*	*Shear*	*Disp.*	*Shear*	*Disp.*	*Shear*	*Disp.*	*Shear*
Design	Abutment A	61.6		108		34		22		81		33		19	
	Top of Pier 1	61.5	3185	102	2389	28	1541	20	1290	75	1984	30	1448	15	1042
	Top of Pier 2	62.1	1472	102	1291	35	834	25	709	81	1074	32	849	22	571
	Top of Pier 3	62.4	1472	103	1249	33	872	23	658	79	1267	31	956	20	503
	Top of Pier 4	[a]	1130	55	1330	23	805	21	717	50	1305	27	904	19	664
	Top of Pier 5	80.9	1148	99	1345	49	745	26	718	57	1221	45	914	20	646
	Top of Pier 6	78.2	1837	90	1537	45	928	23	648	55	369	43	940	19	499
	Top of Pier 7	73.5	4057	84	2257	43	1593	17	1087	52	1700	35	1530	13	962
	Top of Pier 8	68.7	1383	83	1501	44	1304	21	1301	56	1671	39	853	16	1321
	Abutment A	80.6		80		43		19		51		37		16	
	Total shear / Max disp.	**81.7**	**15684**	**108**	**6197**	**49**	**4817**	**26**	**3614**	**81**	**5070**	**45**	**5637**	**22**	**3518**
As-built	Abutment A			67		26		19		49		18		12	
	Top of Pier 1			64	2191	26	1714	15	1425	45	1759	15	1089	9	779
	Top of Pier 2			63	1849	21	1879	21	1116	52	2218	21	974	15	924
	Top of Pier 3			67	1302	24	1250	18	773	50	1299	19	557	11	1044
	Top of Pier 4			62	2394	31	1548	26	2214	55	2769	44	2393	21	2309
	Top of Pier 5			58	2273	18	1676	19	2143	45	1971	23	2410	16	1824
	Top of Pier 6			55	1216	16	773	18	779	43	1158	23	1061	14	822
	Top of Pier 7			47	1638	16	1549	17	1256	40	1864	25	1960	13	1118
	Top of Pier 8			44	2853	25	2837	16	2292	41	2629	29	4235	13	3884
	Abutment A			40		20		19		38		21		17	
	Total shear / Max disp.			**67**	**10289**	**31**	**6261**	**26**	**4578**	**55**	**8474**	**44**	**5864**	**21**	**4051**

Demands are at the pier base (shear) and at the pier top (displacement).

[a] *= 62.6 for Unit 1 and 81.7 for Unit 2 (design displacement demands were monitored in the superstructure).*

Figure 7 confirms that the seismic response in this direction is fundamentally different for the two configurations investigated. For the design assumption, the two units of the bridge have different dynamic characteristics and seismic response. Hence, the displacement time-histories of Unit 1 (Abutment A and Piers 1-3) are different than those of Unit 2 (Pier 5-8 and Abutment B), as shown in Figure 7(a). Pier 4 at the expansion joint has also its distinct response. For the as-built model, the bearing friction couples the two units of the bridge and stimulates the beneficial contribution of Piers 4, 5 and 8 to the lateral force resisting system. It is clear from Figure 7(b) that the displacement response of Unit 1 is comparable to that of Unit 2, with different amplitudes.

Figure 8 depicts a comparison between Fourier spectra of the two configurations investigated obtained from the top acceleration history at Pier 1. Clearly, the inelastic periods of the design assumption are significantly longer than the

as-built bridge. Figure 8(c) pictorially shows the significance of the reduction in period on increasing the seismic loads of the as-built configuration.

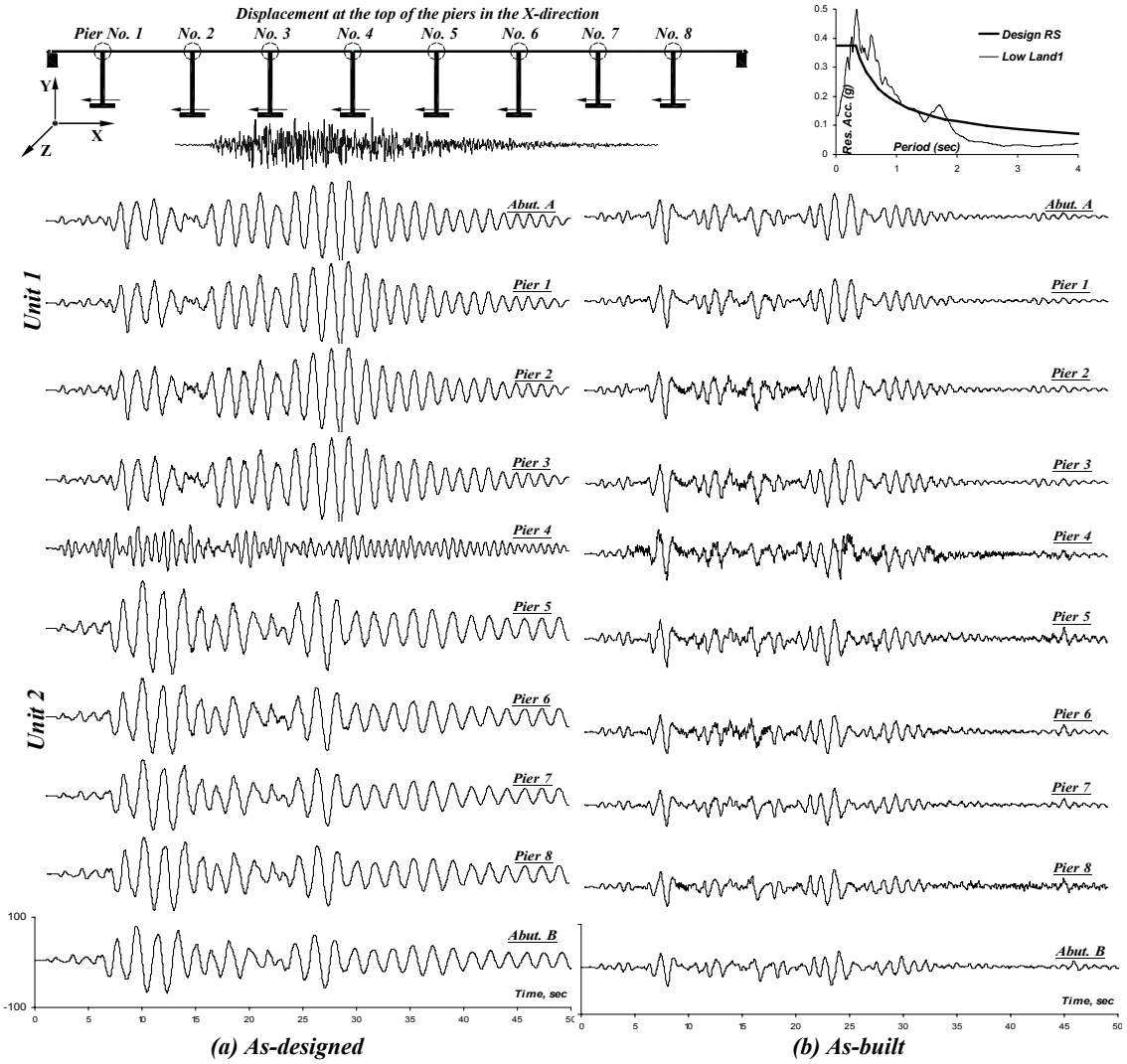

Figure 7. Comparison of displacement histories in the longitudinal direction at the design earthquake (Lowland1).

Comparison of the energy dissipated in different PTFE sliders for the bridge featuring the as-built configuration is pictorially shown in Figure 9. It is clear from the hysteresis loops that the PTFE sliders are able to dissipate large amount of energy under the design earthquake, which results in lower deformation demands compared with the design assumption. It is also shown that the high displacement demand at Abutment A controls the response due to the lower frictional force at this bearing, which is proportional with the normal stresses. The maximum relative

displacement demands at abutments are shown in Figure 7. The demand at Abutment A almost reaches the supply (101.6 mm) for the design configuration. Also, high demands are observed at Abutment B and at the expansion joint. The PTFE bearing frictional resistance significantly reduces these demands in the as-built bridge, particularly at the expansion joint since the two units of the bridge oscillate simultaneously.

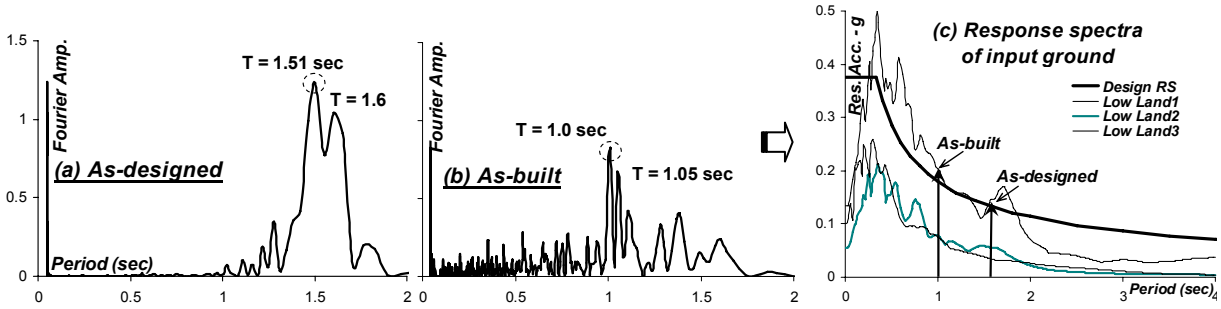

Figure 8. Amplification of seismic forces due to the reduction in period in the longitudinal direction: (a) & (b) Fourier spectra of the response at top Pier 2 for the design and the as-built configurations; (c) response spectra of the input ground motions.

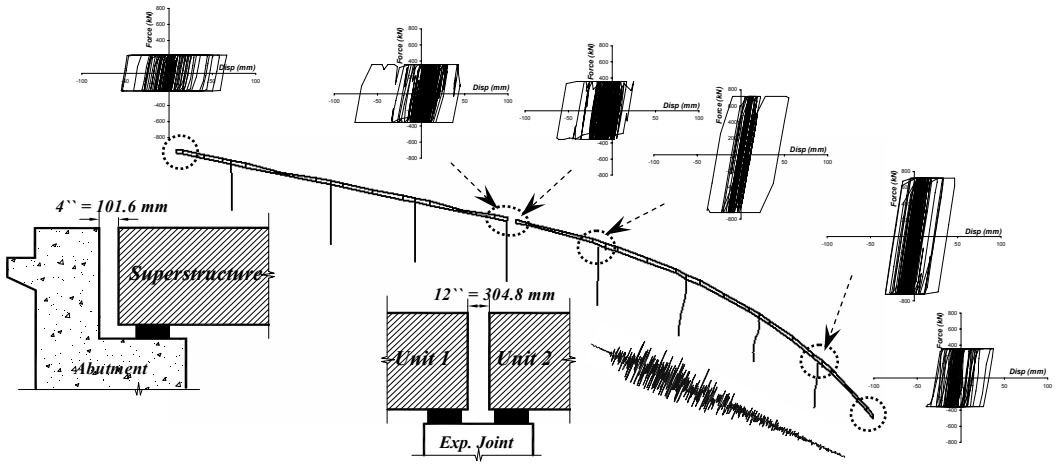

Figure 9. Energy dissipated in PTFE sliders for the bridge featuring the as-built configuration at the design EQ.

Comparisons between the capacity, the design and the base shear demand at the design earthquake for the as-built and the design configuration are shown in Figure 10(a). It is noteworthy that the total design force estimated from

response spectrum analysis is over-conservative since it represents summation of maximum shear forces of various piers, which do not simultaneously occur during the analysis. The realistic summation of base shear time-histories obtained from response history analysis produces significantly lower demands. For both analytical idealizations investigated, the minimum supply is higher than the maximum demand, which is in turn lower than the design.

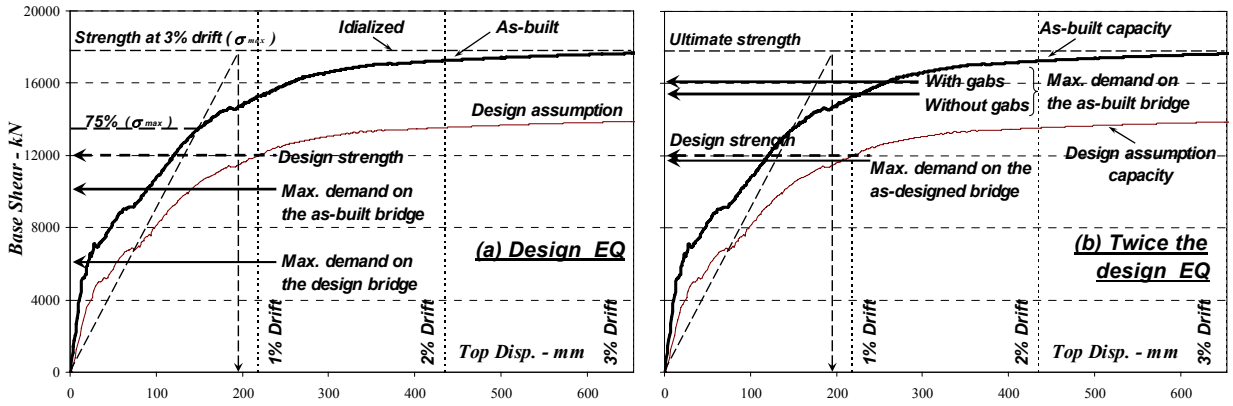

Figure 10. Capacity versus design and demand in the longitudinal direction (design and twice the design EQ).

It is clear from the comprehensive capacity-demand comparisons presented above that the performance of the design assumption in the longitudinal direction is satisfied at the design earthquake for all limit states except for the segment collision criterion. This confirms the conclusions from pushover analysis discussed in the first phase of this study. Including the frictional resistance of PTFE bearings redistributes the displacement demands to the tolerable limits. The performance of the as-built bridge in this direction is therefore satisfactory for all limit states. Nevertheless, it is important to stress that the investigated bridge exhibit high overstrength since the design was governed by flow and ice loads (Mwafy et al. 2006). Therefore, the amplification of seismic forces and base shear demands of the as-built bridge clearly confirms the high uncertainties arising from the assumptions typically used in design of complex bridges.

DEMAND PREDICTIONS AT TWICE THE DESIGN EARTHQUAKE

The results shown at the design earthquake indicated that the maximum demands are generated under the effect of the Blytheville earthquake scenario. The accelerograms generated for this scenario were therefore scaled up to twice the design ground motion and employed to investigate the vulnerability of the bridge under the most credible earthquake. Comparisons between the maximum inelastic demands of the design and the as-built configuration at twice the design earthquake are shown in Table 5.

Response in the Transverse Direction

The bearing friction is more pronounced at this high level of ground motion. It results in a reduction in period and hence higher seismic forces. The demands of the as-built behavior are therefore higher than the as-designed structure. Maximum demands are observed at Pier 4. Displacement demands are 100% higher than those observed at the design earthquake and 300% higher than those used in design. The maximum observed drift at twice the design ground motion is 0.80%, which is quite satisfactory. The maximum relative displacement demands (gap close) in the longitudinal direction at the expansion joint and abutments are shown in Table 5. It is clear that no collision is detected and the margin of safety is satisfactory at this high level of ground motion.

Table 5. Comparison between maximum inelastic displacement and base shear demands of the design and the as-built configuration at twice the design ground motion (*kN - mm*).

Location	***Transverse Direction***						***Longitudinal Direction***								
	Design Assumption			***As-Built***			***Design Assumption***			***As-Built***					
										Without Gaps			***With Gaps***		
	Disp.	*Gaps* [a]	*Shear*	*Disp.*	*Gaps* [a]	*Shear*	*Disp.*	*Gaps* [a]	*Shear*	*Disp.*	*Gaps* [a]	*Shear*	*Disp.*	*Gaps* [a]	*Shear*
Abutment A	24	0.0		29	17		234	191		183	183		181	102	
Top of Pier 1	27		5007	32		5797	226		3895	176		3536	172		3525
Top of Pier 2	79		8555	89		9182	226		3173	189		3272	171		3397
Top of Pier 3	92		5875	105		6198	228		2024	188		2007	176		2172
Top of Pier 4	130	76	7564	158	17	8750	127	187	1754	133	74	1653	140	57	1652
Top of Pier 5	96		5926	97		5947	147		1538	139		1497	127		1529
Top of Pier 6	90		5795	92		6463	140		1631	130		1516	122		1713
Top of Pier 7	49		5506	44		6159	125		1876	121		2925	115		2906
Top of Pier 8	52		5831	48		6982	126		1945	115		1963	115		1924
Abutment B	58	53		42	26		116	116		108	108		105	88	
Total shear / Max disp.	**130**		**33960**	**158**		**35539**	**234**		**11835**	**189**		**15683**	**181**		**16016**

[a]: *Maximum relative displacement (gap close) in the longitudinal direction at the expansion joint and abutments.*

Figure 11 shows the maximum relative displacement demands at abutments and the distribution of plastic hinges of the as-built bridge. A comparison between the global capacity with the maximum base shear demand at this level of ground motion is shown in Figure 6. It is clear that limited inelasticity is generated and the demands are well below the minimum supply. The results confirm the satisfactory performance and the adequate margin of safety in the transverse direction at twice the design ground motion.

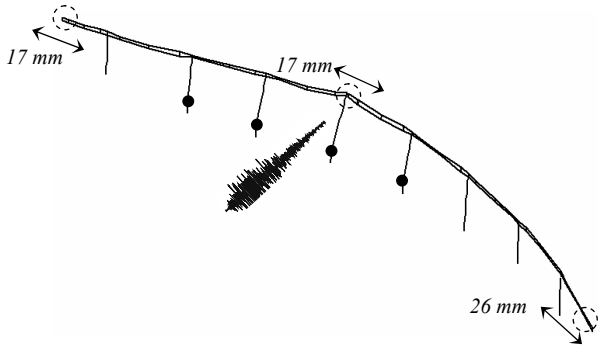

Figure 11. Maximum relative displacement demands of the as-built bridge at the expansion joint and abutments with distribution of plastic hinges (load in transverse direction at twice the design EQ).

Response in the Longitudinal Direction

Comparison between the inelastic demands of the design and the as-built bridge is shown in Table 5. The analysis was conducted for the as-built bridge with and without modeling the structural gaps at abutments and the expansion joint to highlight their significance on the seismic response. The inelastic demands in this direction significantly increase at twice the design earthquake. Although base shear demands exceed the design forces for the majority of substructural elements, no crushing in the concrete core is observed due to the exhibited high overstrength (Mwafy et al. 2006). The response of the design assumption is unacceptable as a result of the high displacement demands, which is almost twice the gap width capacity at abutment A.

The acceptable performance of the as-built structure was shown at the design earthquake. It was confirmed that bearing friction effectively coupled the two units of the bridge and significantly improved the seismic capacity in this direction. It is clear from the response time-histories shown in Figure 12 that the two units of the as-built bridge simultaneously vibrate at twice the design PGA, confirming the significant effect of bearing friction. Modeling the

segment collision at the gaps reduces the displacement demands, while it slightly increases the base shear of few piers, as shown from Table 5. Figure 13 compares between the relative displacement response with and without modeling the gaps at the abutments and the expansion joint. The results confirm the significance of seismic gaps modeling on the response of multi-span curved bridges.

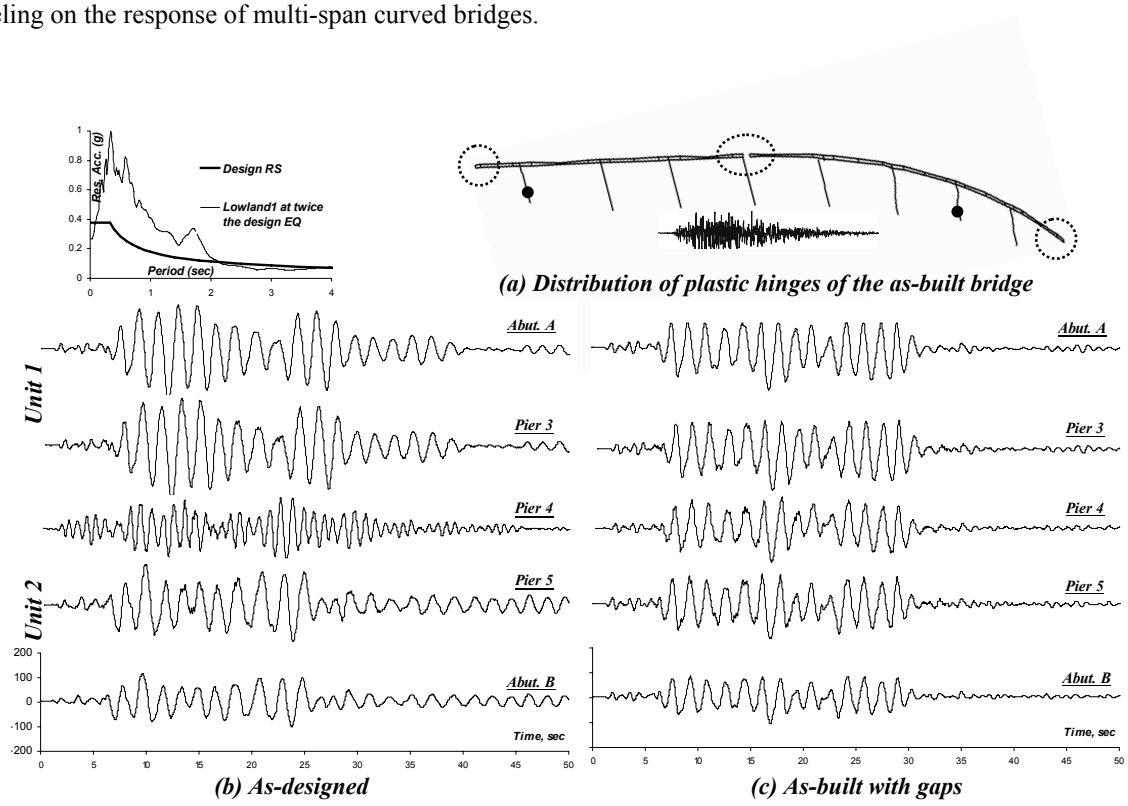

Figure 12. Response in longitudinal direction at twice the design earthquake: (a) mapping of plastic hinges for the bridge featuring the as-built configuration; (b) & (c) comparison of displacement histories for the design and the as-built bridge.

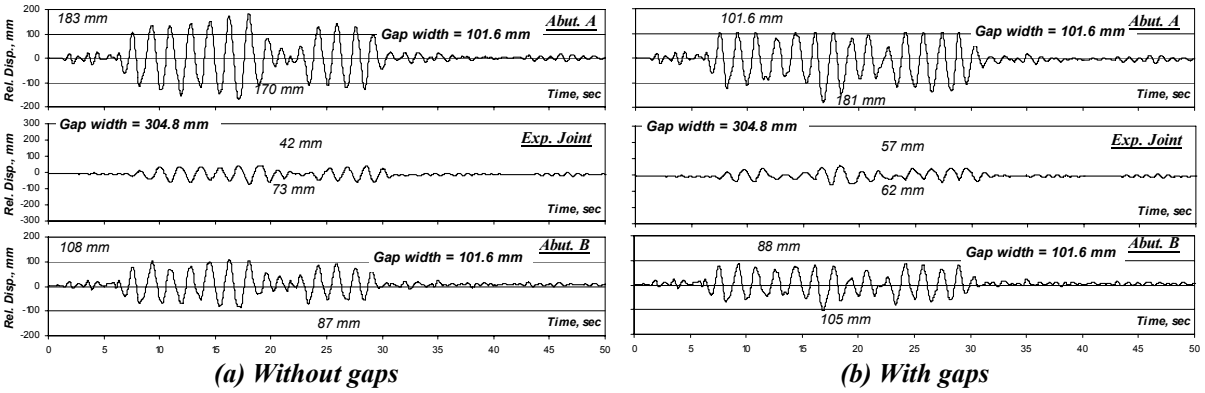

Figure 13. Comparison of relative displacement response in the longitudinal direction at the expansion joint and abutments with and without modeling of gaps (load in longitudinal direction at twice the design EQ).

Comparisons of the capacity to demand ratios of the pinned and PTFE bearings indicate the acceptable response up to twice the design earthquake. For pinned bearings, the superstructure inertia forces are transferred to the substructure through anchor bolts at the top of the piers. The tension and shear capacities of these bolts are 387 kN and 238 kN, respectively. The maximum tension and shear demands on the bolt are 303 kN and 176.7 kN, respectively, which are lower than the capacities. For the PTFE bearings, the maximum seismic demand is 4139 kN., which produces a shear strain of 1.8. This results in a total shear strain lower than the allowable limit recommended by seismic codes and guidelines (e.g. NCHRP 12-49 2001). Also, the maximum displacement demand at the PTFE bearings in the longitudinal direction is lower than the sole plate limits. Hence, no damage is anticipated to the PTFE surface.

Comparison of the overall capacity and maximum base shear demand for the design and the as-built bridge is shown in Figure 10(b). For both configurations, the global demand at twice the design ground motion is slightly below the ultimate capacity. However, the margin of safety of the as-built bridge is lower than the design assumption. Although, controlling the deformation by seismic gaps prevents formation of undesirable modes of failure, it increases base shear demands. The performance of the as-built bridge in the longitudinal direction is therefore satisfactory for all limit states with the exception of the collision at abutments. The results support the conclusions of the first phase of this study and emphasize the significance of pushover analysis procedure in identifying potential structural deficiencies and prioritizing limit state criteria of complex bridges (Mwafy et al. 2006).

CONCLUSIONS

The importance of simplifying design assumptions on the capacity-demand ratio predictions of multi-span curved bridges was investigated in this study. Verification of modeling approaches, prioritizing limit state criteria and comparisons of the dynamic characteristics and capacities of the as-designed and the as-built configurations were addressed in the first phase of the study. The current report presented results of the extensive response history analyses carried out to compare between the inelastic behavior of the two bridge configurations at different levels of ground motion. The following conclusions are drawn based on work reported above:

- In the transverse direction, seismic demands and cracked periods were slightly influenced by bearing friction. This was more pronounced on the curved unit, particularly with increasing the inclination of substructural element. The displacement demands at abutments and the expansion joint though were significantly affected by friction due to the coupling between the two units of the bridge in the longitudinal direction. Maximum displacement and shear demands were 50% higher than the design due to the spectrum amplification in the period range of the bridge. The redistribution of demands when considering bearing friction results in higher margins of safety. The response at the design earthquake was within the elastic range and maximum demands were well below minimum capacities.
- In longitudinal direction, the seismic response of the design assumption was alarming due to the imminent collision at abutments, while it was satisfactory for the as-built bridge due to the uniform distribution of demands. Piers with PTFE sliders effectively enhanced the lateral force resisting system when the bearing friction was considered. Seismic loads though increased due to the considerable reduction in period, which in turn magnified base shear demands. Base shear demands of the as-built configuration were therefore significantly higher (up to 110%) than the design assumption. The results clearly highlighted the high uncertainties arising from the assumptions typically used in design of complex bridges.
- At twice the design earthquake, the safety margins of the as-built bridge in the transverse direction were satisfactory and the structure was just at the onset of the post-elastic range. In the longitudinal direction, the displacement demands increased significantly, while base shear demands exceeded the design forces for the majority of substructural elements. It was confirmed that bearing friction maintained the coupling between the two units of the bridge up to this high level of ground motion. Modeling of structural gaps was significant in analysis. Abutment gaps controlled the displacement demands, which resulted in limited inelasticity at this high level of ground motion. The performance of the as-built bridge in the longitudinal direction was therefore satisfactory for all limit states except for the collision at abutments.

The significance of simplifying design assumptions on the inelastic seismic response of the multi-span complex bridge was confirmed from extensive response history analysis. The results are indicative of other complex bridges. Neglecting bearing friction leads to a possible stiffness reduction in the structural system, resulting in longer periods of vibration. This in turn results in significant reduction in design loads and high uncertainties in the seismic

demand predictions. Assumptions aimed at simplifying the design process may therefore compromise the safety of bridges similar to that studied here. Structural gaps at the abutments controlled the response of the curved bridge in the two principle directions. Attention should be therefore focused on characterizing the behavior of joints and their effect of design actions and deformations. Inelastic response history analysis confirmed and verified the applicability of pushover analysis in identifying structural deficiencies and providing insight into the limit state criteria of multi-span complex bridges at the design and twice the design levels.

ACKNOWLEDGMENTS

This study was funded by the US Federal Highway Administration (FHWA) through the Mid-America Earthquake Center (MAE), University of Illinois at Urbana-Champaign, USA. The Mae Center is an Engineering Research Center funded by the National Science Foundation under cooperative agreement reference EEC 97-01785. The authors are grateful to Professor Glenn Rix, Georgia Institute of Technology, for his advice on earthquake input motions.

REFERENCES

1. AASHTO LRFD Specifications (2005). *AASHTO LRFD bridge design specifications*, 3rd Ed., American Association of State Highway and Transportation Officials, Washington, D.C.
2. AASHTO Standard Specifications (1995). *Standard specifications for highway bridges*, 15th Ed., American Association of State Highway and Transportation Officials, Washington, D.C.
3. Broderick, B.M., Elnashai, A.S., and Izzuddin, B.A. (1994). "Observations on the effect of numerical dissipation on the nonlinear dynamic response of structural systems." *Engineering Structures*, 16(1), 51-62.
4. Chopra, A.K. (2000). *Dynamics of structures: Theory and applications to earthquake engineering*, 2nd ed., Prentice Hall, Englewood Cliffs, New Jersey.
5. Elnashai, A.S., Papanikolaou, V., and Lee, D. (2004). *Zeus-NL - a system for inelastic analysis of structures*, User Manual, Mid-America Earthquake Center, Civil and Environmental Engineering Department, Univ. of Illinois at Urbana-Champaign, Urbana, IL.
6. Elnashai, A.S., and Mwafy, A.M. (2002). "Overstrength and force reduction factors of multistorey reinforced-concrete buildings." *Struct. Design of Tall Buildings*, 11(5), 329–351.
7. Housner G. (1952). Spectrum intensities of strong-motion earthquakes. *Symp. on Earthquake and Blast Effects on Structures*. Los Angeles, Calif. 20-36.
8. Rix, G.J., Fernandez, A., and Foutch, D.A. (2004). "Synthetic earthquake hazard." Project HD-1, Mid-America Earthquake Center, <http://mae.cee.uiuc.edu> (Jan. 31, 06).
9. FHWA (1996). *Seismic design of bridges – Design example No. 5 – Nine-span viaduct steel girder bridge*, US Department of Transportation, Publication No. FHWA-SA-97-010.
10. Mwafy, A.M., Elnashai, A.S., and Yen, W-H. (2006). "Implications of design assumptions on capacity estimates and demand predictions of multi-span curved bridges", ASCE Journal of Bridge Engineering, In Press.
11. Mwafy, A.M., and Elnashai, A.S. (2001). "Static pushover versus dynamic collapse analysis of RC buildings." *Eng. Structures*, 23(5), 407-424.
12. USGS (2002). "Seismic hazard maps for the conterminous U.S. for 2002." U.S. Geological Survey Earthquake Hazards Program, <http://earthquake.usgs.gov> (Jan. 31, 06).